Advances in Physics: X

ISSN: 2374-6149 (Online) Journal homepage: www.tandfonline.com/journals/tapx20

Nonlinear dynamics in breathing-soliton lasers

Junsong Peng, Xiuqi Wu, Huiyu Kang, Anran Zhou, Ying Zhang, Heping Zeng, Christophe Finot & Sonia Boscolo

To cite this article: Junsong Peng, Xiuqi Wu, Huiyu Kang, Anran Zhou, Ying Zhang, Heping Zeng, Christophe Finot & Sonia Boscolo (2025) Nonlinear dynamics in breathing-soliton lasers, Advances in Physics: X, 10:1, 2580628, DOI: 10.1080/23746149.2025.2580628

To link to this article: https://doi.org/10.1080/23746149.2025.2580628

Published online: 16 Nov 2025.

ADVANCES IN PHYSICS: X
2025, VOL. 10, NO. 1, 2580628
https://doi.org/10.1080/23746149.2025.2580628

Taylor & Francis
Taylor & Francis Group

REVIEW ARTICLE

OPEN ACCESS Check for updates

Nonlinear dynamics in breathing-soliton lasers

Junsong Peng[a,b,c], Xiuqi Wu[a,c], Huiyu Kang[a], Anran Zhou[a], Ying Zhang[a], Heping Zeng[a,b,c,d], Christophe Finot[e] and Sonia Boscolo[f,g,h]

[a]State Key Laboratory of Precision Spectroscopyand Hainan Institute, East China Normal University, Shanghai, China; [b]Collaborative Innovation Center of Extreme Optics, Shanxi University, Taiyuan, Shanxi, China; [c]Chongqing Key Laboratory of Precision Optics, Chongqing Institute of East China Normal University, Chongqing, China; [d]Chongqing Institute for Brain and Intelligence, Guangyang Bay Laboratory, Chongqing, China; [e]Universite' Bourgogne Europe, CNRS, Laboratoire Interdisciplinaire Carnot de Bourgogne ICB UMR 6303, F-21000 Dijon, France; [f]Aston Institute of Photonic Technologies, Aston University, Birmingham, UK; [g]VPIphotonics GmbH, Berlin, Germany; [h]Istituto Nazionale di Fisica Nucleare, Laboratori Nazionali del Sud (INFN-LNS), Catania, Italy

ABSTRACT

We review recent advances in the study of nonlinear dynamics in mode-locked fiber lasers operating in the breathing (pulsating) soliton regime. Leveraging advanced diagnostics and control strategies—including genetic algorithms—we uncover a rich spectrum of dynamical behaviours, including frequency-locked breathers, fractal Farey hierarchies, Arnold tongues with anomalous features, and breather molecular complexes. We also identify a novel route to chaos via modulated subharmonic states. These findings underscore the utility of fiber lasers as model systems for exploring complex dissipative dynamics, offering new opportunities for ultrafast laser control and fundamental studies in nonlinear science

ARTICLE HISTORY
Received 26 July 2025
Accepted 21 October 2025

KEYWORDS
Fibre lasers; breathing (pulsating) solitons; nonlinear dissipative structures; synchronization; chaos; smart lasers

1 Introduction

Mode-locked fiber lasers are valued not only as compact sources of ultrashort pulses but also as highly controllable laboratories for nonlinear science. In these cavities, a delicate balance among dispersion, Kerr nonlinearity, and wavelength-dependent gain and loss sustains *dissipative solitons*—localized structures that persist through continuous energy exchange with their environment [1–3]. Because key parameters such as pump power, intra-cavity dispersion, and saturable-absorber characteristics can be tuned with precision, fiber lasers provide an archetypal platform for exploring dissipative dynamics. Their accessible parameter space supports a rich palette of behaviors: breathing oscillations [4–6], soliton explosions [4,7–10], chaotic [11,12] and rogue-wave states [13,14], harmonic mode locking, and self-organized patterns ranging from soliton bunches [15] to stable multi-soliton bound states ("soliton molecules") [16–24]. Many of these phenomena were identified decades ago, yet their underlying physics is only now being elucidated thanks to advanced single-shot diagnostics [25–28] that resolve pulse evolution on a round-trip basis. Insights from these experiments advance fundamental theory—by supplying a testbed for far-from-equilibrium models—and guide practical design, informing the optimization of next-generation ultrafast sources. This dual relevance places mode-locked fiber lasers at the center of contemporary research in ultrafast photonics and nonlinear dissipative systems.

Breathing (or pulsating) solitons, manifesting as localized temporal or spatial structures exhibiting periodic oscillations in energy, are fundamental nonlinear modes observed across a wide range of physical systems. They appear in various domains of natural science, including condensed matter physics [29], fluid dynamics [30,31], plasma physics [32], chemistry, molecular biology, and nonlinear optics [33–35].

CONTACT J. Peng jspeng@lps.ecnu.edu.cn State Key Laboratory of Precision Spectroscopy and Hainan Institute, East China Normal University, Shanghai 200062, China; C. Finot christophe.finot@u-bourgogne.fr Universite Bourgogne Europe, CNRS, Laboratoire Interdisciplinaire Carnot de Bourgogne ICB UMR 6303, F-21000 Dijon, France; S. Boscolo s.a.boscolo@aston.ac.uk Aston Institute of PhotonicTechnologies, Aston University, Birmingham B4 7ET, UK

In conservative systems, breathing solitons can arise spontaneously via modulation instability of continuous waves [29,36–38], owing to the fact that the governing evolution equations—such as the nonlinear Schrödinger equation (NLSE), sine-Gordon equation, or Korteweg-de Vries equation—admit periodic or quasi-periodic solutions [39,40]. In contrast, in dissipative systems such as passive or active optical cavities, breathing solitons typically emerge as limit cycles originating from a steady state through a Hopf bifurcation, also referred to as a Poincaré-Andronov-Hopf bifurcation [41], when system parameters are varied. In optics, dissipative breathers—initially studied experimentally in passive Kerr fiber cavities [42] and microresonators [43–45]—have also emerged as a universal mode-locking regime in ultrafast fiber lasers [6,46,47,48]. In particular, in [6], we reported the first real-time experimental observation of single breathers and breather-pair molecules in a laser cavity using advanced real-time detection techniques. Since then, a series of distinct experimental studies on breather structures in laser systems have been published by various groups (e.g. [49–68]).

This sustained interest is mainly due to two key factors. First, breathing solitons represent a novel mode-locking regime in lasers. Their understanding, characterization, and optimization may open new frontiers in ultrafast laser physics. In particular, self-synchronization phenomena observed in lasers supporting breathing solitons [60,68,69] provide critical insights into ultrafast laser dynamics—knowledge that is essential for the development and practical deployment of next-generation laser systems.

Second, breathing-soliton lasers offer an excellent platform for uncovering novel nonlinear dynamics in dissipative systems. In linear oscillator ensembles, synchronization manifests primarily as phase-locking between coupled modes and is fully described by linear superposition, with each mode evolving independently. In breathing-soliton lasers, synchronization emerges intrinsically from nonlinear coupling among the cavity's internal frequencies, enabling self-synchronization without external forcing. These nonlinear interactions also allow chaotic attractors, which are prohibited in finite-dimensional linear systems, where dynamics are confined to linear combinations of non-interacting eigenmodes and no mechanism exists for intrinsic frequency locking. In this paper, we provide a review of key findings from our recent research in this rapidly advancing field, situating breathing-soliton dynamics within the broader context of nonlinear science. Our aim is not to present an exhaustive survey, but to emphasize conceptual and mechanistic understanding of the breathing-soliton phenomenon, the associated research methods, and the latest advancements, and to delineate how these results advance the understanding of complex dissipative dynamics. These include: the emergence of higher-order Farey hierarchies of frequency-locked breather states and self-similar fractal dynamics [69]; the appearance of abnormal synchronization domains (unusual Arnold tongues) [68]; transitions between synchronized and desynchronized breather regimes, including the identification of a novel intermediate dynamic state [60]; and a new route to chaos through the breakdown of regular dynamics [64]. We also demonstrate the use of genetic algorithms (GAs) to generate breather dynamics with controlled characteristics [56,69].

The paper is organized as follows: Section 2 reviews the key experimental and theoretical tools and methodologies that enable advanced studies of breathing solitons in ultrafast fiber lasers, with an emphasis on real-time diagnostics and GA control. Section 3 examines synchronisation dynamics, including frequency-locked breathers, Farey hierarchies, and Arnold-tongue structures. Section 4 extends this discussion to multi-breather complexes and demonstrates their intelligent control. Section 5 explores transitions of breathing-soliton lasers from regular to chaotic dynamics. Finally, the concluding section summarizes our findings and outlines future research directions.

2 From measurement to model: laser architecture, diagnostics and control strategy

In this section, we review the key tools and methodologies that have enabled the advanced investigation of breathing solitons in ultrafast fiber lasers. Addressing this problem required overcoming several challenges. On the experimental side, substantial progress was achieved through the development of reliable and controllable laser platforms. A critical component was the implementation of appropriate detection techniques, as the non-stationary nature of breathers necessitates diagnostics capable of resolving pulse evolution on a round-trip basis. These measurement capabilities, in turn, facilitated feedback mechanisms for optimizing cavity parameters. To interpret and predict breather dynamics, it was equally important to

compare experimental observations with numerical simulations. For this purpose, we examine two principal modeling frameworks.

It is important to note that this discussion is limited to directly observable breathing solitons. Vectorial structures whose periodic behavior only becomes apparent after polarization analysis [70–73] are not addressed here, as their study necessitates polarization-resolved models. We also exclude regimes associated with dissipative soliton explosions, characterized by abrupt yet quasi-periodic variations in pulse properties linked to Q-switching dynamics [8,10,48].

2.1 Experimental setup

Here, we summarize the key experimental techniques employed for the generation, observation, and control of breathing solitons. Detailed descriptions of setups and methodologies can be found in our previous publications [6,14,54,56,60,69].

2.1.1 Fiber laser architecture

The generation of breathing solitons in fiber lasers does not inherently require cavity designs that differ radically from those used for the generation of conventional ultrashort dissipative solitons. Figure 1 illustrates a typical ring-cavity architecture employed to generate such structures at telecommunication wavelengths (around 1550 nm, within the C band). All components operate in the single-mode regime and are widely available commercially. While the discussion here focuses on a unidirectional ring cavity, breathing solitons have also been observed in figure-eight lasers [64,74], figure-nine lasers [75], linear cavities [76], and Mamyshev oscillators [77], highlighting the universality of the breathing regime beyond a specific laser configuration.

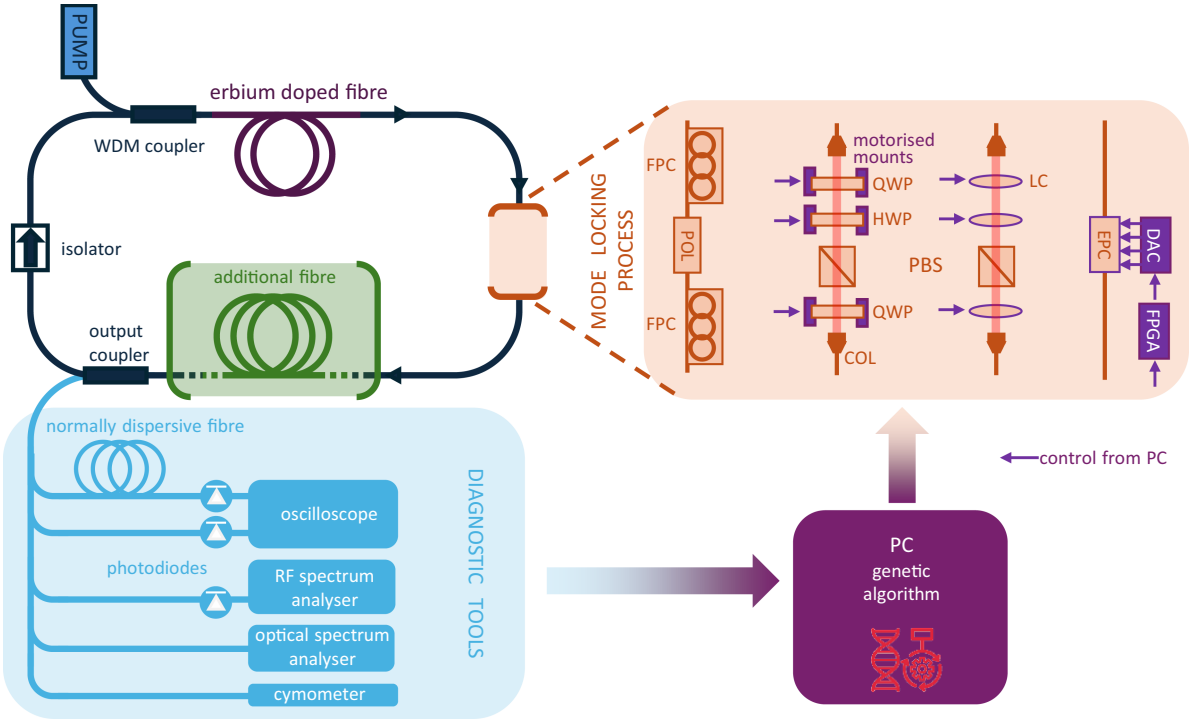

Figure 1. Experimental setup. Schematic of a typical fiber laser cavity used to generate and characterize breathing solitons. The setup includes a set of diagnostic tools for detailed observation of the pulsating structures, as well as passive and active components enabling mode locking via nonlinear polarization rotation. FPC, fiber polarization controller; POL, polarizer; COL, collimator; QWP/HWP, quarter-/half-wave plates; PBS, polarization beam splitter; LC, liquid crystal phase retarder; EPC, electronically driven polarization controller; DAC, digital-to-analog converter.

In the ring-cavity architecture, gain around 1550 nm is provided by an erbium-doped fiber, pumped by a continuous-wave laser diode operating at 976 nm. Although most reported results have been achieved in the C band, oscillatory dynamics have also been demonstrated at other wavelengths, including 1.03 μm, 1.6 μm, 1.7 μm, and 2 μm, using different doped fibers—such as ytterbium-doped [57,74,78–80], erbium-doped [53,81], thulium-holmium co-doped [82], and thulium-doped fibers [83,84]. An inline isolator is typically employed to enforce unidirectional operation, although breathing dynamics have also been reported under bidirectional operation [85]. Polarization control is achieved by incorporating a fiber polarizer or a polarization beam splitter, which ensures maintenance of a single polarization state within the cavity. These components may also be combined in the form of a polarization-dependent isolator. The cavity elements—such as output couplers, pump wavelength-division multiplexers, and isolators—are generally based on standard single-mode fiber, which exhibits anomalous dispersion (typically around -22.8 ps^2/km at 1550 nm). The net cavity dispersion can be finely tuned by inserting segments of normal-dispersion fiber. Breathing dynamics have been observed and characterized in both net-anomalous and net-normal dispersion regimes [46,86], each exhibiting distinct temporal and spectral features. The oscillation period of breathing solitons varies strongly with cavity parameters and pump power—ranging from a few to several tens of cavity round-trips near zero dispersion, to periodicities on the order of hundreds of round-trips in cavities operating under normal dispersion conditions [6].

A fundamental aspect of any ultrashort pulse laser is the mechanism that enables mode locking, particularly the choice and implementation of the saturable absorber within the cavity [87]. This absorber may be a physical component that exploits the intensity-dependent absorption properties of a material [88–90]. However, to circumvent issues such as material degradation and provide greater control and flexibility, *virtual* saturable absorbers can also be employed. In such cases, the Kerr nonlinearity of silica—manifesting through effects like nonlinear polarization rotation (NPR) or phase modulation—is converted into effective intensity modulation by means of polarization filtering or auxiliary optical loops. Ultrafast lasers utilizing NPR [91] have achieved notable success and remain widely used due to their simplicity and high performance. Nevertheless, tuning operating regimes in NPR-based systems has historically relied on manual adjustment of fiber-based polarization controllers or combinations of discrete waveplates. This empirical approach limits reproducibility and stability. To address these limitations, a range of externally controllable polarization management techniques have been developed. These include waveplates mounted on motorized stages [92]; conventional mechanical three-loop fiber polarization controllers enhanced with electronic control [93]; and electronically driven polarization controllers composed of three or four fiber squeezers oriented at 45° with respect to each other [14,56,94,95]. Another approach involves the use of reconfigurable waveplates based on liquid crystal phase retarders in combination with a polarization beam splitter, which can also serve as an output coupler [69,96,97]. In the latter case, the voltages applied to the liquid crystal elements can be precisely controlled via external drivers, enabling rapid and programmable tuning of the polarization state, thus facilitating the efficient exploration of a broad parameter space.

The pulsating (breathing) mode-locking regime typically emerges below the pump threshold for conventional soliton mode locking in normal-dispersion cavities [6], or at higher pump powers beyond the stability range of solitons in cavities with near-zero net dispersion [47,60,64,98].

2.1.2 Diagnostic tools

The characterization of pulses emitted by a breather laser differs fundamentally from that of a conventional mode-locked laser, where identical pulses are emitted on every cavity round-trip. In such conventional systems, both the optical spectrum and the temporal profile can be readily accessed using standard tools such as optical spectrum analyzers or time-domain techniques like optical autocorrelation. The averaged signals produced by these methods faithfully represent any individual pulse. This is not the case for breathing solitons. In these systems, the pulse energy fluctuates from one round-trip to the next. As a result, the electrical signal detected by a photodiode exhibits intensity modulations that reveal period-multiplication dynamics—phenomena observed in non-fiber lasers [99–101] as well as in fiber laser systems [86,102,103]. Figure 2(a) illustrates such oscillatory behavior, showing the round-trip-resolved

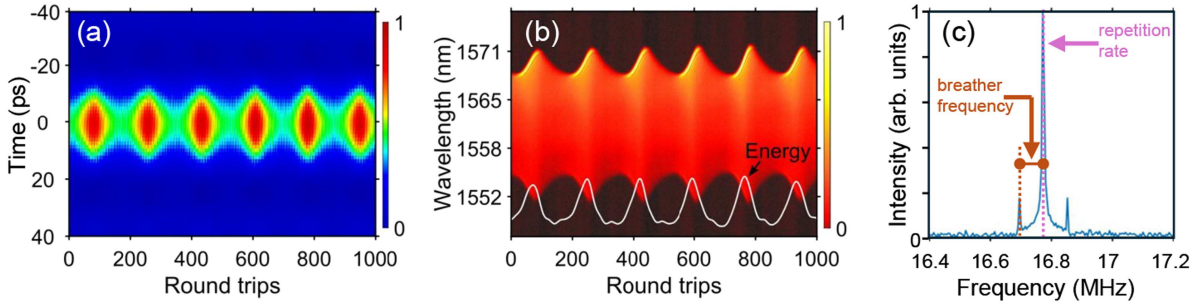

Figure 2. Typical properties of a breathing soliton with a long pulsation period, observed in a laser cavity operating at normal average dispersion. The cavity repetition rate is 16.765 MHz. (a) Temporal evolution of the intensity relative to the average over successive cavity round trips, recorded using a 50-GHz photodiode with a 20-ps response time and a 33-GHz bandwidth oscilloscope operating at an 80-GSa/s sampling rate. (b) DFT measurement of single-shot spectra over consecutive round trips; the white curve indicates the pulse energy evolution. The accumulated dispersion is $-1200\ \mathrm{ps/nm}$, yielding a spectral resolution of 0.025 nm. (c) RF spectrum obtained by Fourier transformation of the photodiode signal. Data adapted from [56], acquired following laser optimization via a GA.

dynamics of a long-period pulsating soliton recorded using a high-bandwidth photodiode and oscilloscope. This measurement employs the spatio-temporal dynamics methodology [104], which consists of recording a long, real-time intensity trace $I(t)$, segmenting it into time windows aligned with cavity round-trips, and assembling these segments into a false-color contour plot. The resulting spatiotemporal map $I(t, z)$ captures the evolution of pulse dynamics over successive round-trips, where the slow coordinate z indexes the round-trip number.

However, current limitations in optoelectronic detection bandwidth restrict access to the full ultrashort temporal features of breathing pulses and may, for example, obscure two closely spaced temporal components. This challenge is overcome using a method known as *time-stretch dispersive Fourier transform (DFT)*, which enables real-time visualization of the spectral properties of individual pulses. DFT has become a breakthrough technique in the characterization of ultrafast events and is now widely adopted by the scientific community [25–28]. The principle of DFT is conceptually analogous to the far-field regime in paraxial diffraction. It relies on the fact that, under sufficient dispersion, the temporal intensity profile of a pulse becomes a stretched replica of its optical spectrum [105]. This linear spectral-to-temporal mapping—typically achieved via propagation through several kilometers of highly dispersive fiber—translates the spectral information into the time domain, enabling direct recording with a fast photodiode and a high-bandwidth oscilloscope. This property has been widely exploited, particularly in the characterization of extreme events and transient laser dynamics [20,21,90,106–108]. Figure 2(b) presents the round-trip-resolved spectral evolution of the same breathing soliton shown in Figure 2(a), captured using the DFT technique. The data clearly show that periodic variations in pulse energy—associated with oscillations in peak amplitude and pulse width in the temporal domain—are synchronized with spectral breathing, i.e. periodic stretching and compression of the optical spectrum.

To obtain a more detailed, real-time full-field picture of the dynamics, DFT can be combined with time-lens techniques that magnify fine temporal structures, making them compatible with the bandwidth limits of available optoelectronics [106,109,110]. DFT is also highly effective for characterizing doublets of closely bound ultrashort pulses, which manifest as sinusoidal modulations in the spectral envelope [6,19,49,88,108,111]. From these spectral modulations, both the temporal delay and relative phase between the constituent pulses can be extracted. When the separation between pulses exceeds several nanoseconds, the optical spectrum of each pulse can even be individually resolved [6,66,112,113]. Moreover, DFT is well suited for analyzing bi-chromatic structures [63]. Furthermore, it has enabled the direct observation of the birth-to-annihilation dynamics of dissipative Kerr cavity solitons in coherently driven Kerr resonators [114], and, when combined with time-lens techniques, has resolved the dynamics of dissipative Talbot solitons in synchronized multicolor fiber lasers [115].

The spectral resolution achieved with DFT allows detection of sharp spectral features such as Kelly sidebands, signatures of four-wave mixing [83,112] or interactions with dispersive waves [116]. It can also reveal periodic shifts in the central wavelength of the breathing soliton [54,81], and has proven essential for

detecting otherwise invisible breathing behavior that is not discernible from pulse energy measurements alone [52]. Today, DFT is such an indispensable tool in the study of oscillatory dynamics that it is difficult to imagine an experimental study in this field without it [27,117].

In conventional mode-locked lasers, the radiofrequency (RF) spectrum primarily provides information about the laser's repetition rate f_r, as well as its noise and timing jitter. In contrast, breather lasers exhibit an additional, defining feature: a pair of sidebands appears symmetrically around the repetition frequency, located at a distance equal to the breathing frequency f_b (see, e.g. Figure 2(c)) [56,62,80,81]. RF measurements can also reveal the coexistence of multiple breathing frequencies, which give rise to trampoline-like dynamics [118,119]. Notably, the sharpness of these spectral features distinguishes this behavior from Q-switching instabilities. As such, the RF spectrum serves not only as a diagnostic tool but also as a valuable input for automated cavity control algorithms. A more detailed physical interpretation of the RF components in breather lasers will be presented in Sections 3 and 4, where their connection to synchronization mechanisms will be established. Finally, high-precision frequency counters (cymometers) may be used to resolve the RF components and evaluate their long-term stability.

2.1.3 Control via genetic algorithms

Despite their fundamental importance, breathing solitons have received comparatively little experimental attention—although this situation is rapidly evolving—primarily because their intrinsic oscillations are difficult to characterize and reproduce in a controlled, repeatable manner. As mentioned in the Introduction, fiber-laser cavities offer numerous tunable degrees of freedom [120], including pump power and small-signal gain [121,122], output-coupler extraction ratio [123], cavity length and average dispersion [124], as well as temporally modulated losses implemented via acousto- [125,126] or electro-optic modulators [127,128]. These parameters define a vast and complex optimization landscape. In practice, the degree of freedom most commonly exploited is the effective saturable absorber. In systems based on nonlinear polarization evolution, this corresponds to tuning the intra-cavity state of polarization, facilitated by the active components described in Section 2.1.1.

The recent implementation of evolutionary and GAs has overcome a major bottleneck by automating exploration of this high-dimensional parameter space. GAs now enable reproducible access to complex operating regimes—such as breathing dynamics—that previously required laborious empirical tuning and whose admissible parameter window is typically narrower than that required for conventional stationary mode locking. The GA approach is particularly well-suited for the global optimization of user-defined targets arising from complex nonlinear interactions—for instance, those involved in supercontinuum generation [129,130]. In photonic cavities, early successes include the automated identification of stationary mode-locked regimes, such as single-pulse [131–133], dual-pulse [134], and harmonic mode-locking states [135]. More recent developments have pushed these so-called *smart lasers* further, demonstrating their ability to self-tune to highly dynamic and complex regimes, including ultra-broadband noise-like emission [92] and the generation of super rogue waves [14].

GAs emulate Darwinian evolution, advancing only the fittest individuals through successive generations [136,137] (see Figure 3(a)). In the present context, an *individual* corresponds to a particular laser operating regime, uniquely specified by the set of control voltages applied to the intracavity polarization controller [56]; these voltages serve as that individual's *genes*. The optimization begins with an initial population whose gene values are random. For every individual, the laser output is evaluated with a user-defined merit (fitness) function, which assigns a quantitative score. A new generation is then created by breeding individuals from the previous generation, with the probability of an individual being selected as a parent weighted by its score. Breeding consists of *crossover*—gene exchange between two parents—to produce two offspring, followed by *mutation*, which randomly perturbs individual genes to maintain genetic diversity. Selection strategy is regime-dependent. For stationary mode-locking, an *elitist* scheme—in which the highest-scoring individuals are cloned directly into the next generation—rapidly preserves desirable traits. By contrast, for breather mode locking, a *roulette-wheel* scheme, which assigns selection probabilities proportional to fitness yet still explores lower-ranking individuals, proves more effective [138] (see Figure 3(b)). Generations iterate until the population converges, yielding the individual (laser setting) that maximizes the fitness function, i.e. the desired operating state.

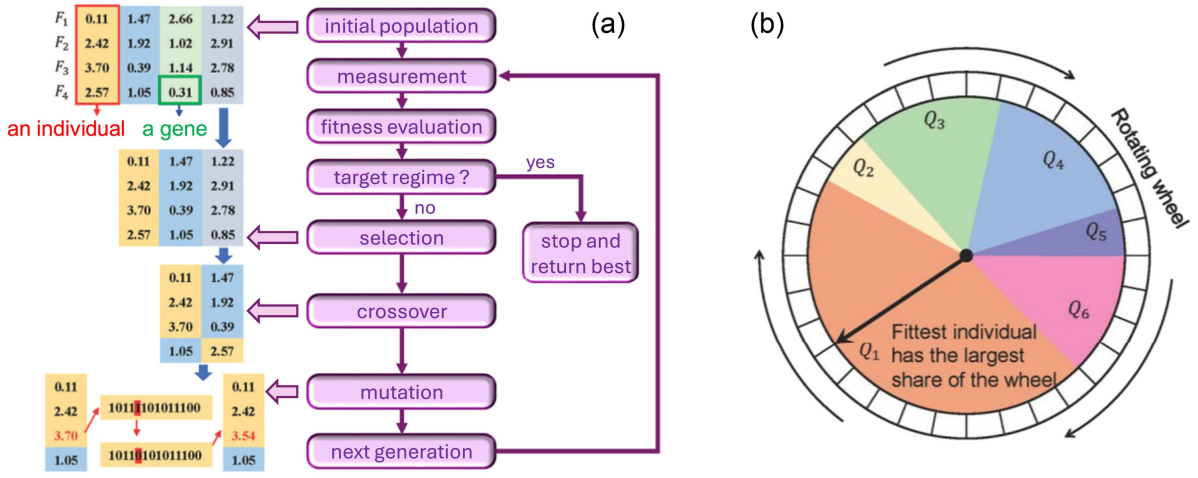

Figure 3. Genetic algorithm principles. (a) Flow chart of the algorithm; (b) "Roulette wheel" selection diagram. Results adapted from [56].

The merit function is the linchpin of any self-tuning scheme: it must increase monotonically as the laser approaches the target state. Simple metrics—such as the peak height at the cavity repetition frequency or the detected pulse count—are effective for locating stationary mode-locked regimes and can be adapted to identify basic breather operation [93]. To reach breather states with prescribed attributes, however, it is advantageous to exploit finer details of the RF spectrum [56]. For an automatically optimized, self-starting breather regime, we define the composite merit function

$$F_{\mathrm{merit}} = \alpha F_{\mathrm{ml}} + \beta F_{\mathrm{b}}, \qquad F_{\mathrm{b}} = 1 - \sum_{f_{\mathrm{r}}-\Delta}^{f_{\mathrm{r}}+\Delta} I(f) \Big/ \sum_{f_{-1}}^{f_{+1}} I(f), \tag{1}$$

where F_{ml} quantifies the quality of mode locking and is taken as the average pulse intensity [93,132]. Its role is to penalize operating states—such as noise-like pulsing or relaxation oscillations—that can mimic breather spectra. The second term F_{b} discriminates between stationary and breathing operation. In a breather, the modulation frequency f_{b} appears as symmetric sidebands $f_{\pm 1}$ around the cavity repetition frequency f_{r} [$f_{\mathrm{b}} = |f_{\pm 1} - f_{\mathrm{r}}|$; see Figure 2(c)]; in a stationary mode-locked state, these sidebands are absent. Accordingly, F_{b} is constructed from the ratio of the spectral power at f_{r} (summed over a window of width 2Δ) to the power contained in the sideband region spanning f_{-1} to f_{+1}. The weighting coefficients α and β are chosen empirically. By augmenting F_{merit} with additional terms, we have obtained fine control over breather attributes such as the breathing ratio and period [56]. When the pump power is set high enough to favor multi-pulse self-starting, the same composite merit function—followed by a pulse-count constraint—enables the GA to stabilize breather molecular complexes with a user-specified number of constituent breathers, as demonstrated in Section 2.1.3. A further refinement exploits the defining hallmark of *frequency-locked* breathers, namely the high signal-to-noise ratio (SNR) at the breathing sidebands [Figure 4(a3-a4)]. Incorporating this SNR metric into F_{merit} proved essential for directing the GA to laser states that exhibit precise frequency locking, thereby allowing systematic exploration and tailoring of the Farey-tree hierarchy of locked ratios reported in Ref. [69] and discussed in Section 3.2.

This area is undergoing rapid development on both the algorithmic and hardware fronts [139–141]. Emerging control strategies—most notably those that integrate neural-network (NN) [142,143] surrogates with evolutionary search—are markedly improving optimization speed and accuracy, even as the dimensionality of the parameter space grows. These advances are now enabling real-time tuning of increasingly intricate mode-locking regimes that were previously beyond practical reach.

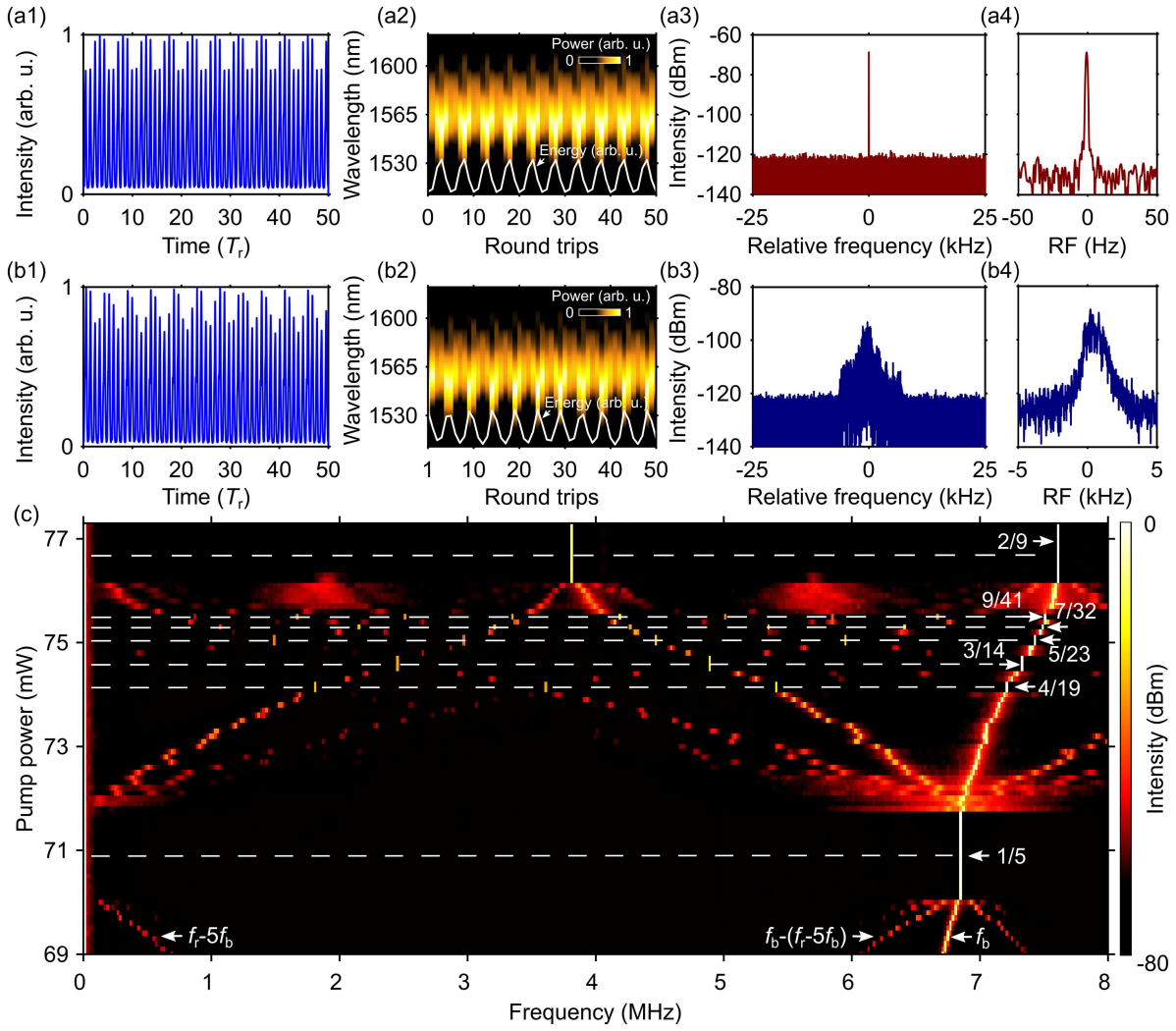

Figure 4. (a, b) Experimental characterization of synchronized and unsynchronized breathing-soliton states. (a1, b1) Photodetected DFT signals captured over consecutive cavity round trips (T_r denotes the round-trip time). (a2, b2) Corresponding single-shot DFT spectra; white curves trace the energy evolution. (a3-a4, b3-b4) Associated RF spectral measurements. The synchronized state (a3-a4) shows a single-mode oscillation at the subharmonic breathing frequency over spans of 50 kHz and 100 Hz. In contrast, the unsynchronized state (b3-b4) exhibits unstable multimode oscillation of a non-subharmonic breathing frequency over 50-kHz and 10-kHz spans. The reference frequency corresponds to one-fifth of the fundamental repetition rate. (c) Experimental observation of frequency locking: RF spectrum of the laser output versus pump power, showing the sequential emergence of rational winding numbers. Adapted from [69].

2.2 Laser model

In this section, we present and discuss the two principal physical models that have underpinned the conceptualization and characterization of pulsating solitons as a distinct class of nonlinear dissipative structures. While these models remain foundational for physical insight, the rapid development of machine learning (ML) has recently introduced alternative approaches, particularly those based on NN architectures of varying complexity [144–146]. Although these data-driven models offer promising avenues—especially due to their high-speed simulation capabilities after training—they typically require a substantial dataset for training, often generated numerically. Moreover, their "black-box" nature can obscure the underlying physics, making it difficult to interpret the contribution of individual components. Despite these limitations, such approaches are increasingly valuable for complementing traditional modeling strategies, particularly when navigating high-dimensional or experimentally inaccessible regimes.

2.2.1 Master-equation approach based on the cubic-quintic Ginzburg-Landau equation

To investigate the dynamics of fiber lasers and assess the generality of experimentally observed behaviors, a widely adopted approach is to perform numerical simulations based on the master equation formalism—one of the foundational methods in the theory of passively mode-locked lasers. Originally introduced by Haus [147], this framework has evolved into the cubic-quintic Ginzburg-Landau equation (CQGLE), which is often considered the minimal-complexity model that still supports soliton solutions. In its standard form, the CQGLE is expressed as

$$i\Psi_\xi + \frac{D}{2}\Psi_{\tau\tau} + |\Psi|^2\Psi + \eta|\Psi|^4\Psi = i\Theta\Psi + i\epsilon|\Psi|^2\Psi + i\beta\Psi_{\tau\tau} + i\mu|\Psi|^4\Psi, \tag{2}$$

where Ψ is the normalized complex envelope of the optical field, τ denotes the normalized time in a reference frame moving at the group velocity, and ξ represents the propagation distance along the unfolded cavity. The dimensionless temporal and spatial coordinates are scaled by a characteristic pulse duration T_0 and the dispersion length $L_D = T_0^2/|\bar{\beta}_2|$, respectively, where $\bar{\beta}_2$ is the path-averaged group-velocity dispersion of the cavity. On the left-hand side of Eq. 2, the parameter $D = -\mathrm{sgn}(\bar{\beta}_2)$ indicates the sign of the dispersion regime, and η quantifies the quintic nonlinear refractive index contribution. The right-hand side contains the dissipative terms: Θ represents the net linear gain or loss, β is the gain bandwidth parameter, and ϵ and μ are the cubic and quintic gain/loss coefficients, respectively.

The master-equation framework is invaluable for discerning the spectrum of nonlinear structures that can emerge in an optical cavity [1]. Beyond stationary dissipative solitons, the CQGLE predicts *pulsating* solitons—periodic attractors that occupy an intermediate state between stationary behavior and chaos [86,148]. In phase space, stationary solitons correspond to fixed points, whereas pulsating solitons trace limit cycles [149]. The CQGLE also reproduces extreme breathing dynamics [5], eruptive structures [4], soliton pairs (molecules) exhibiting vibrational oscillations, and compound breathing states [6,54,58]. Moreover, it captures routes to chaos via successive bifurcations [86,148]. Because key physical parameters such as dispersion, gain, and saturation enter explicitly, the model readily accommodates higher-order linear and nonlinear effects [150–153]. Although the CQGLE is most often integrated numerically, reduced-order solutions can be obtained via moment methods [149,153,154] or variational techniques employing trial functions [155], reinforcing its versatility as a universal model for dissipative systems.

2.2.2 Lumped model based on the generalized nonlinear Schrödinger equation

Despite the considerable success of the CQGLE in providing a qualitative and descriptive understanding of the main families of solutions that can arise in fiber lasers, it remains challenging to apply this approach when accurate quantitative agreement with experimental observations is required. Consequently, a more reliable modeling framework for optimizing fiber cavity design has progressively gained attention. This challenge has been addressed through a *lumped modeling* approach, wherein each section of the fiber cavity is modeled individually. Unlike the CQGLE framework—whose parameters are difficult to relate directly to the physical characteristics of specific cavity segments—the lumped model enables straightforward incorporation of experimentally measured values, thereby improving the fidelity of simulations. Moreover, it offers valuable physical insight into the nonlinear pulse dynamics occurring within each segment or component of the cavity.

As previously noted, by focusing in this study on pulse regimes that do not involve periodic energy exchange between polarization modes, a scalar approximation is sufficient to describe light propagation in the fiber. The generalized NLSE is used to model the pulse evolution in each fiber segment [87]:

$$\psi_z = -\frac{i\beta_2}{2}\psi_{tt} + i\gamma|\psi|^2\psi + \frac{g}{2}\left(\psi + \frac{1}{\Omega^2}\psi_{tt}\right), \tag{3}$$

where $\psi = \psi(z, t)$ denotes the slowly varying electric field envelope, t is the retarded time, and z is the longitudinal propagation coordinate. The coefficients β_2 and γ represent second-order dispersion and Kerr

nonlinearity, respectively. The dissipative terms account for linear gain as well as a parabolic approximation of the gain spectral profile, with bandwidth Ω. The gain is modeled as a saturable function given by $g(z) = g_0 \exp\left(-\frac{E_p}{E_{sat}}\right)$, where g_0 is the small-signal gain (nonzero only in the gain fiber), $E_p(z) = \int dt \mid \psi \mid^2$ is the pulse energy, and E_{sat} is the saturation energy determined by the pump power. More advanced gain dynamics can also be implemented, particularly to account for the population dynamics of the active ions in the doped fiber [63,90], and to provide insight into Q-switching-related regimes.

The NPR-based mode-locking mechanism can be modeled using an instantaneous and monotonically increasing nonlinear transfer function applied to the field amplitude:

$$T = \sqrt{1 - q_0 - q_m / \left[1 + \frac{P(t)}{P_{sat}}\right]}, \tag{4}$$

where q_0 denotes the unsaturated loss of the absorber, q_m is the saturable loss (modulation depth), $P(z, t) = \mid \psi(z, t)\mid^2$ is the instantaneous pulse power, and P_{sat} is the saturation power. Linear losses—accounting for intrinsic fiber losses and output coupling—are typically imposed after the passive fiber segments.

The numerical model is generally solved using a symmetric split-step Fourier method [156]. To improve convergence towards the nonlinear steady-state structure, simulations often begin with a Gaussian-like initial condition rather than random noise. It is worth noting that the inclusion of higher-order dispersive terms, such as fourth-order dispersion, has revealed the potential existence of pulsating quartic solitons [157–160].

3 Synchronization dynamics

First identified by Christiaan Huygens in 1665 [161], frequency locking—or synchronization—is the process by which coupled nonlinear oscillators adjust their frequencies to match or maintain a rational ratio (known as the winding number). This phenomenon is ubiquitous across both natural and engineered systems, appearing in contexts as diverse as biological clocks, chemical reactions, mechanical and electrical oscillators, and lasers, to name just a few well-known examples [162]. It underpins a broad range of technologies, including telecommunications, global navigation systems, and biomedical instrumentation. Recently, laser cavities and microresonators operating in the breathing-soliton regime have emerged as a compelling platform for investigating synchronization dynamics within a single physical system [45,47,60,69]. In these systems, harmonics of the breathing frequency f_b can lock to the cavity repetition frequency f_r, driven by nonlinear coupling and competition between the intrinsic system frequencies, with f_r acting as the master and f_b as the slave. This self-synchronization mechanism obviates the need for external modulation or auxiliary resonators, offering a compact and inherently robust approach to frequency locking. In the following, we demonstrate that breathing-soliton lasers serve as enabling platform for the emergence of intricate synchronization phenomena and the manifestation of self-similar fractal dynamics in nonlinear systems.

3.1 Different breather states

As discussed in the Introduction, mode-locked lasers can support not only stationary dissipative solitons but also breathing solitons, depending primarily on the pump strength and the intra-cavity polarization state, the latter effectively modulating the cavity loss [6,47,54,56,60,61,63,69]. The transition from stationary to breathing solitons is associated with a Hopf bifurcation—a widely observed dynamical instability marking the onset of periodic behavior in nonlinear systems. Figure 4(a) and 4(b) illustrate two distinct breather regimes that emerge at closely spaced pump powers: a subharmonically synchronized (frequency-locked) breather state, and an unsynchronized (quasi-periodic) state [69]. In the synchronized regime [Figure 4(a1–2)], the photo-detected signal after time stretching, optical spectrum, and pulse energy

exhibit strictly periodic variations with a well-defined period—5 cavity roundtrips in this case—indicative of subharmonic entrainment. By contrast, the quasi-periodic regime [Figure 4(b1–2)] displays degraded temporal and spectral periodicities. The most prominent distinction between the two regimes is evident in the corresponding RF spectra [Figure 4(a3–4, b3–4)]. The synchronized state exhibits a sharp breathing frequency component with narrow linewidth (0.5 Hz) and a high SNR, precisely located at one-fifth of the cavity repetition frequency, yielding a rational winding number $f_b/f_r = 1/5$. Conversely, the unsynchronized state is characterized by a broadened, noisy breathing frequency that deviates from this rational subharmonic. Direct time-resolved measurements of the breathing frequency using a cymometer reveal marked disparities in frequency stability between the two regimes [69]. As explored further in the following subsection, the locked breathing frequency remains robust over a range of pump power values, indicating the presence of a synchronization plateau.

The distinct characteristics of the two breather states are also evident in the pump-power-resolved RF spectrum shown in Figure 4(c), which captures the onset and evolution of frequency locking. At lower pump powers, three dominant RF components are observed: the breathing frequency, the difference frequency between f_r and the 5th harmonic of f_b ($f_r - 5f_b$), and the difference frequency between the first two ($6f_b - f_r$). As $f_r - 5f_b$ approaches zero, the system undergoes a transition to a locked state with a winding number of 1/5. Further increases in pump power induce redshifts in this winding number, giving rise to a sequence of rational ratios and indicating the emergence of a devil's staircase structure characteristic of frequency-locking transitions in nonlinear systems, as discussed in the next subsection. Notably, the observation of breather frequency locking requires the net cavity dispersion to be close to zero; such dynamics are absent when the laser operates under moderate or large normal dispersion [6]. In the latter case, the breathing frequency is comparatively slow, leading to RF spectra densely packed around f_r (see, e.g. Figure 2(c)) and to sidebands that are not located exactly at subharmonics of f_r. This reflects that the breathing oscillation is not readily commensurate with the cavity round-trip time. By contrast, near-zero dispersion yields much faster breathing oscillations—by an order of magnitude or more (cf. Section 2.1.2)—which are easily subharmonically related to f_r and therefore capable of frequency locking. This distinction highlights the fundamentally different physical mechanisms underlying the two breathing-soliton regimes [163].

Our further investigations [60] have revealed the existence of an intermediate state between the synchronized and unsynchronized phases of breather structures, which we refer to as the *modulated subharmonic state*. To the best of our knowledge, this regime has not been previously observed in nonlinear systems. A characterization of this state—distinguished by a self-modulation of the subharmonically synchronized breather oscillations—is presented in Section 4.2.

3.2 Farey tree and devil's staircase

Frequency locking has been studied across a wide range of physical systems, including charge-density waves [164], Josephson junctions [165], and the Van der Pol oscillator [166], among others [167]. The distribution of frequency-locked states in parameter space—exhibiting the fractal structure known as the devil's staircase [168,169]—can be understood through the number-theoretic framework of Farey trees [170–173]. The Farey tree is a hierarchical sequence of rational numbers constructed via the Farey-sum (or mediant) operation, denoted by $\oplus$: given two adjacent fractions, $\frac{m}{n}$ and $\frac{p}{q}$, a new fraction is generated at the next level of the tree by summing the numerators and denominators separately, yielding $\frac{m}{n} \oplus \frac{p}{q} = \frac{m+p}{n+q}$. In the context of nonlinear dynamics, the Farey tree provides a framework for understanding the local organization of two-frequency resonances. The physical motivation for its use lies in the observation that, between two adjacent resonances, the Farey fraction—with the smallest denominator—is typically the dominant resonance in that interval. This hierarchical structure gives rise to a devil's staircase curve composed of an infinite number of plateaux, exhibiting characteristic self-similarity and fractal geometry.

In optics, frequency-locking phenomena have been extensively studied in externally modulated semiconductor lasers [174–178], where tuning the modulation frequency allows direct observation of the Farey

hierarchy and the devil's staircase structure [175]. Frequency locking has also been observed in a range of other systems, including coupled or externally driven Kerr resonators [179,180], coupled semiconductor laser oscillators [181], fiber lasers with externally modulated loss [125,126] or gain [154], solid-state lasers operating in dual-mode regimes [182], and in the generation of soliton-pair molecules in solid-state lasers under external modulation [183]. In all of these cases, synchronization is driven by an auxiliary oscillator or an external modulation source that introduces a distinct characteristic frequency into the system. In contrast, optical resonators supporting breathing solitons inherently exhibit two characteristic frequencies, thereby offering a fundamentally different platform for studying frequency locking without external forcing.

In [69], by systematically exploring transitions between different breather states in a laser cavity accessible via pump-power tuning, we reported, for the first time, a high-order Farey tree hierarchy of frequency-locked states. Figure 5(a) shows a representative measurement of the breathing frequency as a function of pump power, starting from the region corresponding to a winding number of 1/5 (see Figure 4). The data reveals a characteristic devil's staircase structure, with distinct plateaux. The frequencies corresponding to the plateaux can be associated with rational winding numbers, as identified through the analysis of the RF spectra [Figure 5(b)]. In each frequency-locked state, the RF spectrum displays a finite number n of equally spaced sidebands below the cavity repetition rate f_r. The most prominent line corresponds to the breathing frequency f_b, and if this line is the m-th component from the low-frequency side, then the associated winding number is given by $f_b/f_r = m/n$. Remarkably, the winding numbers emerge sequentially across the pump power axis in the order prescribed by the Farey tree [inset of Figure 5(a)], with the width of each plateau inversely correlated with the level at which the corresponding fraction m/n appears in the Farey hierarchy. The gaps in pump power between adjacent steps (plateaux) correspond to regions of quasi-periodic breather oscillations, similar to the example shown in Figure 4(b).

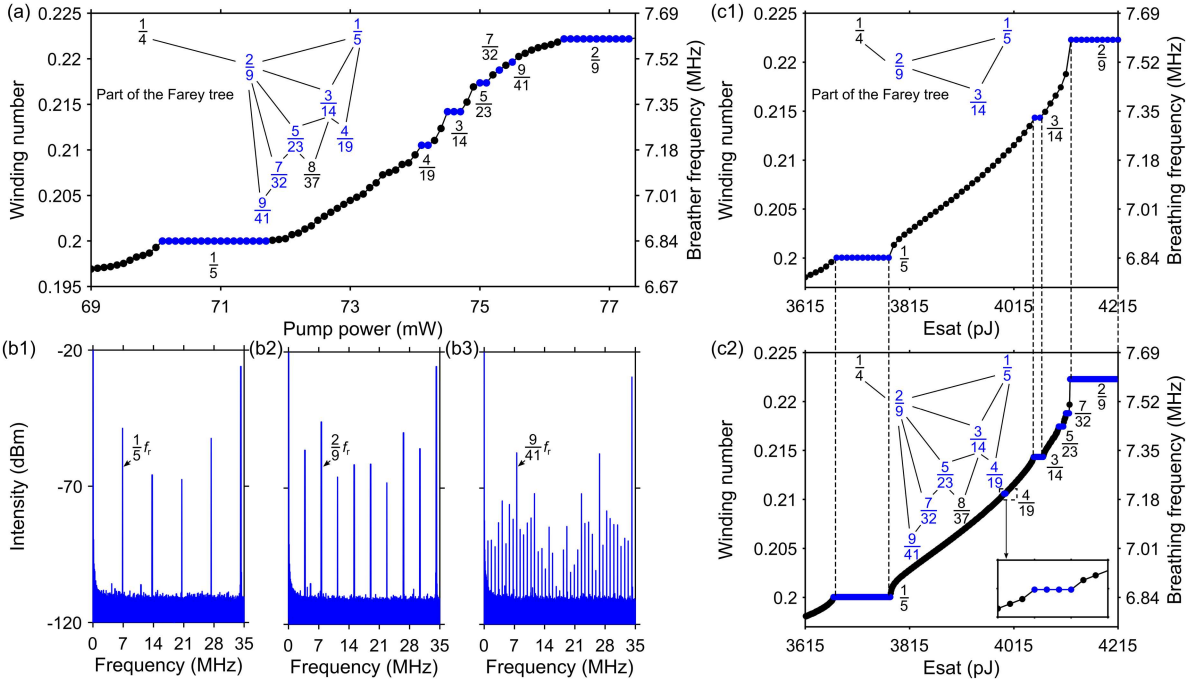

Figure 5. Farey tree and devil's staircase. (a) Measured breathing frequency (winding number) plotted as a function of pump power. The inset shows the relevant portion of the Farey tree, with the observed winding numbers highlighted in blue. (b) RF spectra corresponding to frequency-locked states with winding numbers 1/5, 2/9, and 9/41, respectively. In each case, a set of equidistant spectral lines emerges within the frequency span defined by the cavity repetition rate f_r = 34.2 MHz. (c) Simulated breathing frequency (winding number) as a function of the gain saturation energy, varied with step sizes of 10 pJ and 1 pJ, respectively. The finer step reveals additional plateaux, indicating a fractal structure in the frequency-locking behavior. Insets display the relevant sections of the Farey tree with the observed Farey fractions. Adapted from [69].

The fractal dimension D of the staircase, calculated from the distribution of these gaps [184], is found to be $D = 0.906 \pm 0.025$—closely approaching the theoretical value of 0.87 predicted for a complete devil's staircase, as described by the circle map model [168], thereby highlighting the universal nature of frequency-locking dynamics in nonlinear systems governed by two competing frequencies.

A remarkable feature emerging from Figure 5(b) is that the frequency-locked breather regime gives rise to the excitation of dense RF combs—e.g. 41 times denser than those produced in the standard single-pulse stationary regime in the case of Figure 5(b3). Notably, the line spacing in these combs is not constrained by the cavity length and can extend into the sub-MHz range. As a stable alternative to long fiber cavities, such lasers hold strong potential for applications like high-resolution spectroscopy.

Figure 5(c) presents the corresponding numerical simulation results, showing the breathing frequency as a function of the gain saturation energy, which plays a role analogous to the pump power in the experiment (cf. Section 2.2.2). The parameter is varied starting from the range corresponding to the 1/5 locked state, using two different step sizes. With finer steps, a larger number of frequency-locked plateaux emerge, confirming the fractal nature of the winding number distribution. As shown in Figure 5(c2), the model successfully reproduces the same portion of the Farey tree observed in the experiment, spanning breathing frequencies from 1/5 to 2/9. Moreover, the gaps between the steps in gain saturation energy resemble those found experimentally in pump power. The fractal dimension of the gap set calculated from the model is $D = 0.873 \pm 0.009$, which is even closer to the theoretical value expected for a complete devil's staircase—thanks to the ability of the model to use arbitrarily small increments in gain saturation energy.

A slight change in the initial polarization state of the laser in the experiment—or equivalently, a slight variation in the intracavity loss in the model—can trigger the emergence of Farey fractions from different branches of the Farey tree [69]. Our simulations further demonstrate that the frequency-locking phenomenon is robust across a wide range of laser parameters, including net cavity dispersion and the modulation depth of the saturable absorber [185]. More recently, experiments using a figure-nine laser configuration [75] and dispersion tuning to induce Farey-tree locking [186] have reinforced the robustness and universality of the fractal dynamics observed in breather lasers. These findings have also stimulated analogous investigations into self-synchronization phenomena in Kerr resonators [187] and fractal dynamics in terahertz quantum cascade lasers [188].

3.3 Complexity of Arnold tongues

In the classical master-slave synchronization scheme described by Adler's equation, the frequency of the slave oscillator locks to that of the master when their frequency detuning lies within a specific range [162,189]. This locking range expands with increasing coupling strength, forming a characteristic tongue-shaped region—commonly referred to as an *Arnold tongue* after mathematician Vladimir I. Arnold [190]—in the parameter space defined by frequency detuning and coupling strength. Within this region, both frequency and phase locking are achieved. Arnold tongues serve as a fundamental tool for controlling synchronization dynamics, which is essential for practical applications. These structures have been extensively investigated across diverse physical systems, including coupled nanomechanical oscillators [191], Kerr resonators [192,193], biological oscillators [194,195], oscillators subjected to external frequencies [196], and many others [197–199]. Additionally, Arnold tongues have been observed in the synchronization of the internal dynamics of soliton molecules in fiber lasers under external modulation [127].

Although Arnold tongues are considered universal features of synchronization, pioneering theoretical studies have shown that, under sufficiently strong forcing, the locking region may cease to broaden with increasing drive strength, leading to a significant deviation from the classical tongue shape [162,200]. Instead, the region first widens and then narrows, evolving into a distinct leaf-like structure [200]. Additionally, strong forcing can give rise to *holes* within Arnold tongues—regions of quasi-periodic (unsynchronized) dynamics embedded within the synchronized domain—as demonstrated in theoretical studies of flow systems [201]. Although not explicitly addressed, similar dynamical behavior was also implied in theoretical studies of breathing solitons in optical microresonators [45]. However, experimentally accessing these nonstandard regimes remains challenging, as many real-world synchronized systems become fragile under strong forcing. In optical systems, for instance, a strong external drive from the

master oscillator can disrupt the delicate coherent pulsing states of the slave oscillator [127,179,181]. This phenomenon, known as *amplitude death*, refers to the complete suppression of oscillations under excessive forcing [162,202,203]. In contrast, resonators supporting breathing solitons inherently exhibit a significant imbalance in strength, with the master oscillations (f_r) being much stronger than the slave oscillations (f_b)—thus creating a favorable platform for exploring abnormal synchronization regimes. In [68], by implementing high-resolution control of intra-cavity loss (via a neutral density filter) to modulate the coupling strength between f_b and f_r in a breather laser—thereby introducing a second degree of freedom alongside the pump strength used to characterize the frequency-locking range—we demonstrated that this intrinsic asymmetry provides experimental access to synchronization dynamics that deviate from the canonical Arnold tongue structure. Specifically, we revealed both a leaf-like and a ray-like pattern—of which the former had previously only been studied numerically in the circle map model [200]—and experimentally observed both for the first time. In addition, we identified holes within Arnold tongues, marking the first experimental confirmation of this theoretically predicted feature [201].

Figure 6(a) presents an example of a synchronization pattern observed in our laser. The synchronization region is clearly resolved in the map of breathing frequency intensity across the parameter space defined by pump current and intra-cavity loss [Figure 6(a1)], where it exhibits a distinct leaf-like shape, highlighted by the blue dashed outline. To better visualize this structure, the corresponding locking range is plotted as a function of pump current in Figure 6(a2). In addition to the main synchronization region corresponding to a winding number of $f_b/f_r = 1/5$, two narrower synchronization regions also emerge in Figure 6(a1), associated with winding numbers 3/14 and 2/9. These three ratios follow the Farey tree ordering (cf. Section 3.2). The black areas in Figure 6(a1) indicate either stationary soliton states or continuous-wave laser operation.

Interestingly, the synchronization region in Figure 6(b1–2)—obtained under different polarization controller settings—exhibits a fish-ray-like structure, with a 'head' that contains a distinct 'hole', as highlighted in the insets. This hole reflects a transition from synchronized breather oscillations to an unsynchronized state, followed by re-entry into synchrony as the pump current is tuned. To illustrate this, a cross-section of the inset in Figure 6(b1) is shown in Figure 6(b3), where the drop in breathing frequency intensity corresponds to points within the hole. The breathing frequency's variation with pump current, plotted in Figure 6(b4), reveals a nearly parabolic dependence between two synchronization plateaux—a feature also predicted theoretically in breathing soliton dynamics within microresonators [45]. Such holes have been linked to quasi-periodic states [201], which is confirmed experimentally by the phase diagram in Figure 6(b5), characteristic of quasi-periodic dynamics [162,204,205]. For comparison, the phase diagram of the synchronized state in Figure 6(b6) displays five fixed points, consistent with the winding number 1/5.

These unconventional synchronization patterns were also reproduced in our lumped laser model within the parameter space of gain saturation energy and intra-cavity loss, with all key features—including the holes—closely mirroring those seen in the experiment [68]. Notably, the high-resolution parameter sweeps required for this analysis were made computationally feasible through the use of parallel computing. Numerical simulations have confirmed that the transmission function of the NPR plays a central role in shaping the synchronization regions within the system. Furthermore, these simulations have revealed the complex dependence of the locking range on intra-cavity loss. Notably, in regimes of high loss—where the slave becomes substantially weaker than the master—the foundational assumptions of Adler's weak-injection theory [189] no longer hold.

While the physical origin of the "holes" appearing within otherwise continuous synchronization regions remains unresolved, both our experimental and numerical results indicate that such features can only be observed under conditions of precise control over both linear and nonlinear intra-cavity losses. This finding may inform future experimental strategies in other nonlinear photonic systems, such as microresonators [206].

4 Breather complexes: control and synchronization of composite structures

The interaction between optical solitons can give rise to compact and stable self-assembled bound states, commonly referred to as *soliton molecules* [16–24]. These entities display striking analogies to matter

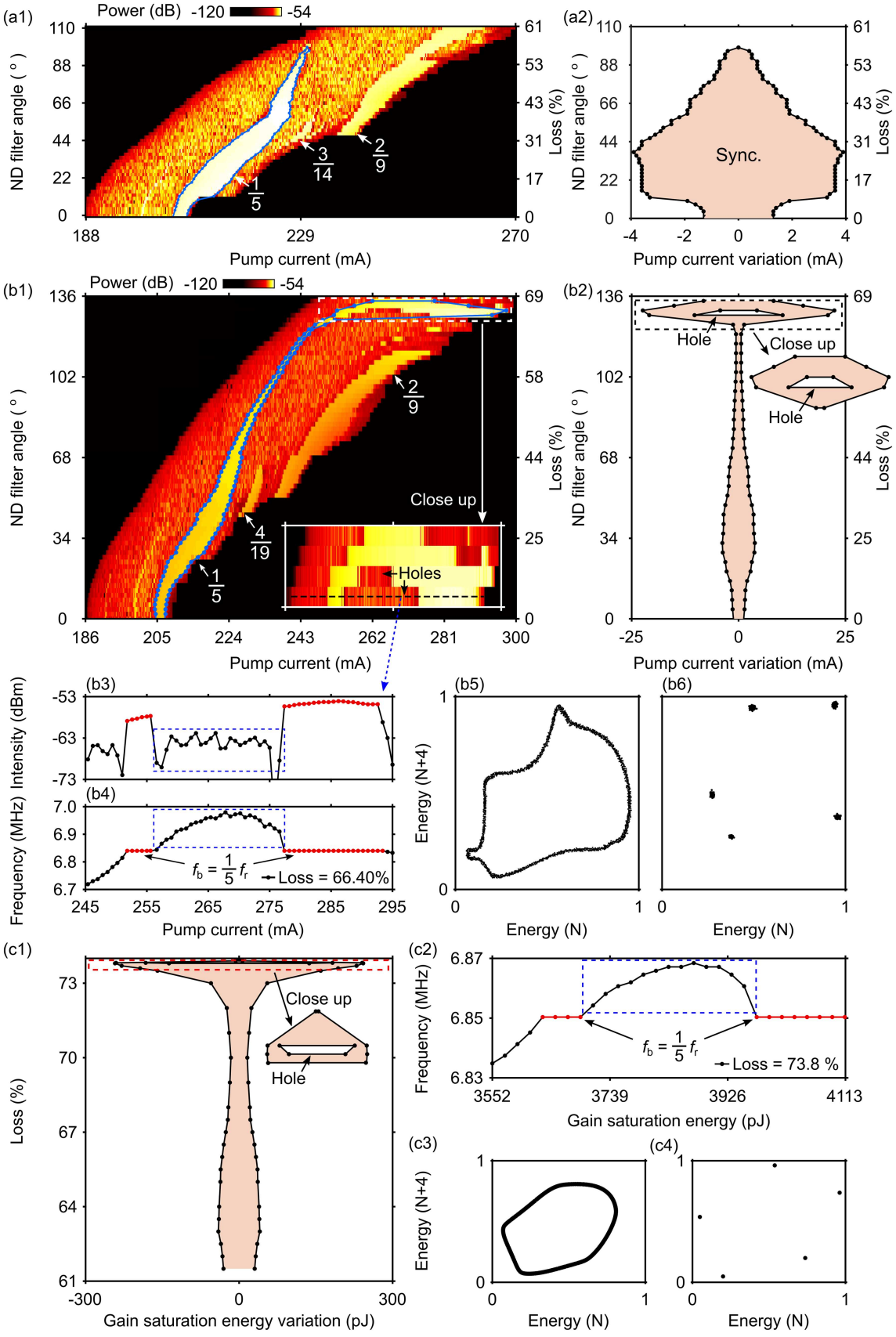

Figure 6. Leaf-like and ray-like synchronization regions observed in the experiment. (a1, b1) Maps of the breathing frequency intensity in the parameter space defined by pump current and intra-cavity loss (the latter controlled via rotation of a neutral density filter). Regions enclosed by blue dashed contours correspond to high-intensity signals and denote the

(caption on next page)

main synchronization regions, associated with a winding number of $1/5$. (a2, b2) Synchronization regions extracted from (a1) and (b1), respectively, highlighting their distinct leaf-like and ray-like structures. For clarity, the pump current axis at each loss value is offset relative to the midpoint of the corresponding plateau in (a1, b1). Synchronized and unsynchronized states are indicated in pink and white, respectively. The dashed rectangular areas in (b1) and (b2) are magnified in the corresponding insets. (b3) Cross-section of the inset in (b1), showing a drop in breathing frequency intensity between two plateaux (red markers). (b4) Corresponding variation of the breathing frequency with pump current. (b5, b6) Poincaré sections for unsynchronized and synchronized states, respectively, showing the phase portraits of pulse energy at cavity roundtrip $N + 4$ versus N. Adapted from [68].

molecules, with properties such as formation dynamics, intrinsic vibrational modes, and switching behaviors. Soliton molecules are pervasive in ultrafast lasers and passive nonlinear resonators, where multiple traveling pulses can interact over extended temporal scales. While soliton pairs constitute the fundamental building blocks of such assemblies, higher-order molecular complexes are also possible, including macromolecules, soliton crystals [207–210], and even highly ordered supramolecular arrangements through engineered long-range interactions [211]. Remarkably, although breathing solitons are fundamentally distinct from stationary ones, recent studies have demonstrated that they can also exhibit collective behavior akin to molecular organization [6,44,49,50,53,58,59,62,65,66]. In [6], using real-time temporal and spectral measurements of a normal-dispersion mode-locked fiber laser, we reported the first experimental observation of breathing soliton-pair ("diatomic") molecules in lasers. This study was expanded in [54], where we demonstrated a variety of breather molecular complexes in an anomalous-dispersion cavity by tuning the intra-cavity loss at fixed pump strength. These included multi-breather (tetratomic) molecules, as well as hybrid assemblies formed by the binding of two diatomic molecules or of a diatomic molecule with a single breather. A key finding was that the inter-molecular temporal separations in these breather complexes exceeded those in stationary soliton molecules [22] by more than an order of magnitude. This observation is consistent with the presence of long-range interactions [212] mediated by slowly decaying dispersive waves radiated in the anomalous-dispersion regime [213]. Additionally, we observed rich non-equilibrium dynamics within these complexes, including breather collisions and the annihilation of individual breathers.

In this section, we demonstrate the automatic generation of breather molecular complexes with a controllable number of constituent breathers within a laser cavity, enabled by the use of GAs [56]. Furthermore, we extend the study of synchronization phenomena to include multi-breather complexes [60], uncovering new pathways for manipulating their collective dynamics.

4.1 Intelligent dynamics generation

While soliton molecules in fiber lasers can be generated simply by raising the pump power above the fundamental mode-locking threshold—with the number of solitons in each molecule scaling monotonically with the pump power [19,22]—the excitation of breather molecules is more challenging. Moreover, in normally dispersive fiber cavities, the formation of multi-breather complexes (more than two breathers) is hindered because breathers propagating in the normal-dispersion regime do not emit dispersive waves [6]. To circumvent this limitation, we recently introduced a GA strategy that optimizes the highly dynamic breathing behavior of ultrafast lasers by exploiting distinctive features in the RF spectrum of the breather output (see Section 2.1.3 and Ref. [56]). Using this approach, we accessed a broad family of breather molecular complexes exhibiting diverse internal dynamics. Representative results are collected in Figure 7. In particular, Figure 7(a) displays two examples of breather-pair molecules, showing the round-trip evolution of their DFT spectra, first-order single-shot optical autocorrelation traces obtained via Fourier transformation of those spectra, and the relative phases between the constituent breathers extracted from the autocorrelation data [22]. Figure 7(a1) displays a dense fringe pattern in the single-shot spectra, exhibiting a pronounced Moiré effect. The very small fringe spacing corresponds to a large intramolecular pulse separation of 268 ps, as confirmed by the autocorrelation trace in Figure 7(a3). The relative phase, $\phi_{2,1}$, between the trailing and leading breathers evolves almost linearly with the number of round-trips [red curve, Figure 7(a4)]. Because the phase-evolution slope is proportional to the intensity

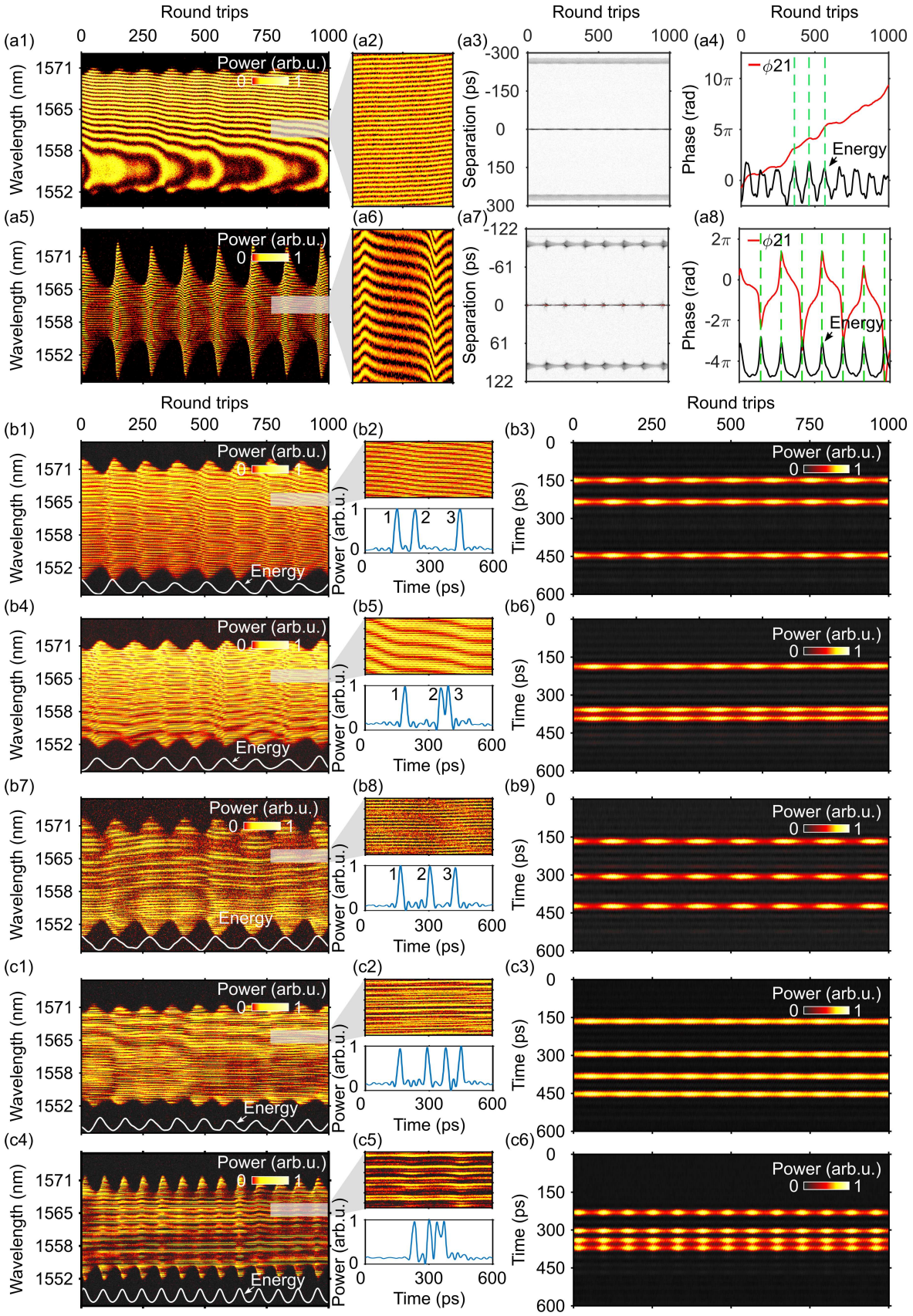

Figure 7. Genetic-algorithm-optimized breather molecular complexes containing two, three, and four breathers. (a) Diatomic molecules. Two archetypes are shown: an *increasing-phase* pair (top row) and an *oscillating-phase* pair (bottom row). (a1,a5) DFT recordings of single-shot spectra over successive cavity round trips; the dense Moiré fringe pattern in

(caption on next page)

(a1) indicates a large intramolecular pulse separation. (a2,a6) Magnified views of the DFT data. (a3,a7) First-order single-shot autocorrelation traces versus round-trip number. (a4,a8) Evolution of the relative phase between the two breathers (red) and of the total molecule energy (black). (b) Breather triplets. Results for a (2 + 1) complex, a (1 + 2) complex, and a triatomic molecule. (b1,b4,b7) DFT single-shot spectra; white curves trace the total intra-cavity energy. (b2,b5,b8) Enlarged spectral windows together with the corresponding temporal-intensity profiles. (b3,b6,b9) Temporal-intensity evolutions referenced to the average round-trip time. (c) (1 + 3) complexes. Examples with (top) large and (bottom) small internal pulse separations. (c1,c4) DFT single-shot spectra. (c2,c5) Close-up spectral views and associated temporal intensities. (c3,c6) Temporal-intensity evolutions relative to the average round-trip time. Adapted from [56].

difference between the two bound pulses [18,19], this linear trend implies an essentially constant intensity imbalance, with the trailing breather remaining the more intense of the pair throughout the evolution. By contrast, the molecule in Figure 7(a5–a8) exhibits a markedly broader breathing of the optical spectrum, an intramolecular pulse separation reduced by nearly a factor of three, and a strongly oscillatory relative-phase dynamics. The phase modulation in Figure 7(a8) signals continuous energy exchange between the two breathers: the pulses attain equal intensity and the total intracavity energy peaks at the round-trip indices where the phase-evolution curve reaches its extrema.

Extending the discussion beyond di-breather molecules, Figure 7(b) summarizes GA-optimized solutions for three archetypal bound-breather triplets: a (2 + 1) complex, in which a di-breather molecule precedes a single breather; a (1 + 2) complex, where the single breather leads the di-breather; and a triatomic molecule comprising three nearly equidistant breathers. The DFT-based single-shot spectra and the corresponding spatio-temporal intensity maps differ markedly among these cases, and these contrasts govern their internal phase and energy dynamics. As shown in [56], in the (2 + 1) and (1 + 2) complexes, the relative phases evolve almost linearly with round-trip number: the central pulse is the weakest, while the trailing pulse is strongest in the (2 + 1) configuration; the opposite hierarchy holds for the (1 + 2) configuration, where the leading pulse dominates. By contrast, the triatomic molecule exhibits an oscillatory phase evolution. Figure 7(c) shows the dynamics of two representative (1 + 3) breather complexes. The spatio-temporal intensity evolutions in panels (c3) and (c6) reveal markedly different pulse separations within the two complexes, highlighting the diversity of their structural configurations. As with the previously discussed cases, more targeted measurements allow us to resolve the internal motion of these complexes in detail and to discern the distinct dynamical behaviors that emerge [56]. These behaviors contrast significantly with those typically observed in stationary soliton molecular complexes, underscoring the richer and more complex internal dynamics accessible in breather-based systems.

4.2 Synchronization, desynchronization and intermediate regime

Building on the investigation of single-breather synchronization discussed in Section 3, in [60] we demonstrated, for the first time, the occurrence of subharmonic synchronization and desynchronization of multi-breather molecule-like bound states within a laser cavity. As noted in Section 3, we additionally identified an intermediate regime—modulated subharmonic breathing—that emerges between the synchronized and desynchronized phases. Our results underscore the inherent robustness of the phase transition, demonstrating that it persists independently of the number of constituent breathers forming the soliton structure. This finding further supports the universality of synchronization and desynchronization phenomena in nonlinear systems and opens new avenues for investigating the dynamics of systems involving three or more interacting frequencies [214,215].

Figure 8(a) presents a typical evolution of the RF spectrum of the laser emission as a function of pump current. At low currents (up to 102 mA), the laser emits a single soliton pulse per cavity round trip, marked by a single frequency component at the cavity repetition frequency f_r= 33.39 MHz (not visible in Fig. 8(a), where a reduced frequency span is used for clarity). Increasing the pump current induces a Hopf bifurcation, leading to the generation of a breathing soliton with a pulsation period of four round trips, as evidenced by the emergence of a narrow subharmonic peak at $f_b = f_r/4$, indicating frequency locking [69]. Further pump increase drives the laser into the so-called *modulated subharmonic* regime [60], distinguished by the appearance of additional, symmetrically spaced spectral lines around f_b. The spacing

between these lines corresponds to a longer pulsation period in the time domain, forming a characteristic 'modulated subharmonic' RF structure. Beyond 106 mA, the frequency locking is disrupted: the modulated sidebands vanish and f_b begins to drift continuously with pump current, becoming non-commensurate with f_r. At currents exceeding 111 mA, the pulsating behavior gives way to brief chaotic dynamics, followed by the formation of diatomic stationary-soliton molecules up to approximately 117 mA. Subsequent increases introduce breathing-soliton molecules, with alternating subharmonic, modulated subharmonic, and non-harmonic regimes observed between 117–133 mA. Beyond 133 mA, the system transitions to triatomic breather molecules, repeating the same RF spectral evolution. Figure 8(a) also reveals an important trend: as the number of elementary constituents increases, the subharmonic breather structures exhibit enhanced robustness against variations in pump strength.

Complementary spatio-spectral measurements of the laser dynamics across the three phases are summarized in Figure 8(b), using the diatomic breather molecule as a representative example. Qualitatively similar behavior was observed for the triatomic breather molecule regime [60]. Panels (i–iii) show roundtrip-resolved optical spectra acquired via the time-stretch technique. The subharmonic and non-subharmonic regimes exhibit strictly periodic and degraded periodic variations, respectively, in both the optical spectrum and pulse energy across successive round trips [cf. Figure 4(a2, b2)]. In both cases, the period of spectral fringes remains nearly constant, indicating a stable intra-molecular pulse separation. By contrast, the modulated subharmonic regime features two distinct periodicities: a short

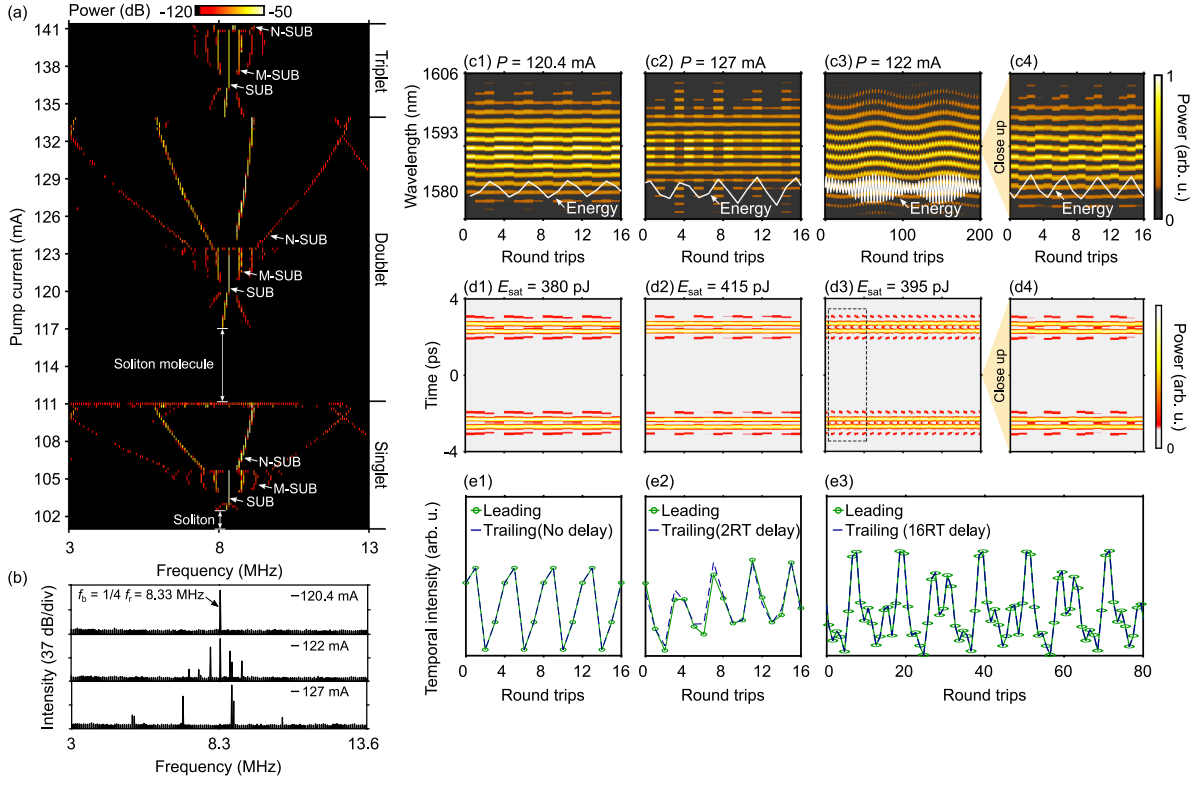

Figure 8. Synchronization dynamics and regimes of breathing-soliton structures. (a) Measured RF spectra of the laser output as a function of pump current, illustrating a sequence of dynamical transitions from subharmonic (SUB) to modulated subharmonic (M-SUB) and finally to non-subharmonic (N-SUB) states. These transitions are observed for single breathers as well as for diatomic and triatomic breather molecules. (b1–b3) DFT recordings of single-shot optical spectra over consecutive cavity round trips, corresponding to SUB, N-SUB, and M-SUB regimes in diatomic breather molecules, respectively. The overlaid white traces depict the pulse energy evolution. (b4) Magnified view of (b3), highlighting short-period breathing dynamics. (c) Representative RF spectra for the three breathing regimes. (d1–d3) Simulated temporal intensity evolutions over successive round trips for SUB, N-SUB, and M-SUB diatomic breather molecules. (d4) Magnified view of (d3). (e) Evolution of peak intensities for the leading and trailing pulses in the three breather molecule regimes. In the N-SUB and M-SUB states, the trailing pulse has been delayed by a fixed number of round trips to demonstrate lag synchronization between the two breathers. Adapted from [60].

period of 4 roundtrips and a long modulation period of approximately 88 roundtrips. The corresponding RF spectra around $f_r/4$ [Figure 8(c)] further highlight the distinctions among the three regimes: the subharmonic state exhibits a single, extremely narrow frequency component located exactly at $f_b = f_r/4$; the modulated subharmonic state displays a symmetric set of narrow sidebands around $f_b = f_r/4$; while the non-subharmonic regime presents broadened spectral lines, consistent with frequency-unlocked laser operation [69].

The RF spectral intensity as a function of the gain saturation energy, obtained from simulations of the laser model (cf. Section 2.2.2), showed excellent agreement with experimental observations [60]. Crucially, the simulations—providing full access to the underlying temporal dynamics—unveiled that in the unsynchronized and modulated subharmonic regimes, the constituent breathers within a soliton molecule are mutually synchronized with a constant time delay, exhibiting *lag synchronization* [162,216,217]. This behavior is illustrated in Figure 8(d, e), where the roundtrip evolution of the temporal intensity profiles and the peak intensities of the leading and trailing pulses reveal a consistent delay between the two breathers [panels (d2–3)]. When this delay is numerically compensated for, the evolution of the pulses becomes fully synchronous [panels (e2–3)]. Similar lag synchronization behavior was also observed in triatomic breather molecules. Moreover, the temporal profiles [Figure 8(d)] highlight a recurring structural feature across the three breather molecule states: each breather is composed of multiple sub-pulses, indicative of higher-order soliton-like evolution within the anomalous dispersion segment of the laser cavity.

By adjusting the laser's polarization state in the experiment (equivalent to varying intra-cavity loss in the model), we also identified direct transitions between synchronized and desynchronized states, consistent with saddle-node bifurcations [162]. These dynamical transitions resonate with broader analogies in the field of dissipative soliton physics, where nonlinear fiber lasers have been shown to exhibit behaviors reminiscent of states of matter—such as soliton molecules, crystals, rains, and gases [218]. In this context, the synchronization-desynchronization dynamics of breathing solitons and their bound states can be qualitatively linked to commensurate-incommensurate phase transitions [219], a class of phenomena well-known in condensed matter physics and other complex systems.

5 Transition to chaos and the modulated subharmonic route

Theoretical studies have shown that solitons can exhibit chaotic behavior in perturbed systems [12,220–222]. While experimental observations have so far been largely restricted to spin-wave systems [223,224], the possibility of chaos driven by optical solitons remains a subject of considerable interest. Chaotic solitons offer a natural extension of laser chaos [225] into the framework of the generalized NLSE, and this extension is significant for two main reasons. First, the generation of chaos within the Maxwell-Bloch formalism generally requires external signal injection [226] or impractically high pump powers, whereas soliton chaos can arise spontaneously in free-running mode-locked lasers, as predicted in [12]. Second, a wide range of physical systems are known to follow three well-established universal routes to chaos: the Ruelle-Takens scenario via quasi-periodicity [227], the Feigenbaum scenario via period-doubling [228], and the Pomeau-Manneville scenario via intermittency [229]. These classical routes are typically described by Lorenz-type systems or one-dimensional maps. In contrast, the generalized NLSE is fundamentally different and may enable novel pathways for the transition from regular to chaotic dynamics. Identifying such mechanisms in real systems governed by the NLSE or its extensions is therefore of fundamental importance in the broader context of nonlinear science.

Despite the significance of soliton chaos and early theoretical predictions in mode-locked lasers [12], experimental studies of optical chaotic solitons have remained limited—primarily due to ultrafast dynamics that exceed the temporal resolution of conventional electronic detection systems. Consequently, earlier experiments were unable to unambiguously confirm the presence of soliton chaos [230], a challenge similarly encountered in Kerr resonator systems [231]. However, a recent study [232] has provided the first systematic experimental evidence of soliton-to-chaos transitions in a mode-locked laser, following a route marked by cascaded short- and long-period pulsations, as revealed through RF spectral analysis and

Lyapunov exponent evaluation. More recently, this same scenario of cascaded pulsations has also been observed in the internal dynamics of soliton-pair molecules [233].

In [64], we employed real-time measurements to reveal a new pathway from solitons to chaos, wherein the transition occurs via the modulated subharmonic state of a breather laser described in the previous section. This route to chaos—referred to as the *modulated subharmonic route*—was unambiguously identified in both experiments and numerical simulations, and its universality was demonstrated across two distinct laser architectures: figure-eight [234] and ring-cavity configurations.

Figure 9 summarizes the experimental results obtained using a figure-eight laser setup. As shown in panels (a) and (b), the characteristic RF sidebands of the modulated subharmonic state drift with increasing pump power and have a noisy structure. These unstable sidebands [64] ultimately give rise to chaos, as indicated by the emergence of a significantly broadened RF spectrum. To validate the chaotic behavior, we computed Poincaré maps, Lyapunov exponents, and correlation dimensions of the reconstructed phase space [204,235]. Figure 9(c) presents the sequence of Poincaré sections corresponding to the laser operating states shown in Figure 9(b). In the subharmonic breather state (panel I), the phase portrait exhibits six fixed points, which evolve into open loops in the modulated subharmonic state (panel II). These loops become connected by scattered points (panel III), indicating an expansion of the phase space and the onset of chaos. In the fully chaotic regime (panel IV), this structure is further broadened. Notably, the Poincaré section in panel III retains periodic components—evidenced by open loops—coexisting with a certain amount of chaotic motion, a hallmark of the so-called *chaotic resonance* predicted in [12]. This mixed state is also reflected in the RF spectrum [Figure 9(b), III], where a dominant peak indicates periodicity, while the surrounding broadband noise signifies chaos. It is also worth noting that the phase portraits were reconstructed using pulse energies derived from the single-shot optical spectra measured via DFT. In contrast, attempts to extract similar phase-space information from direct temporal intensity measurements—without time-stretch—failed to resolve the attractor structure due to the limited temporal resolution of the photodetector, which could not capture the soliton duration (∼ 665 fs) [64].

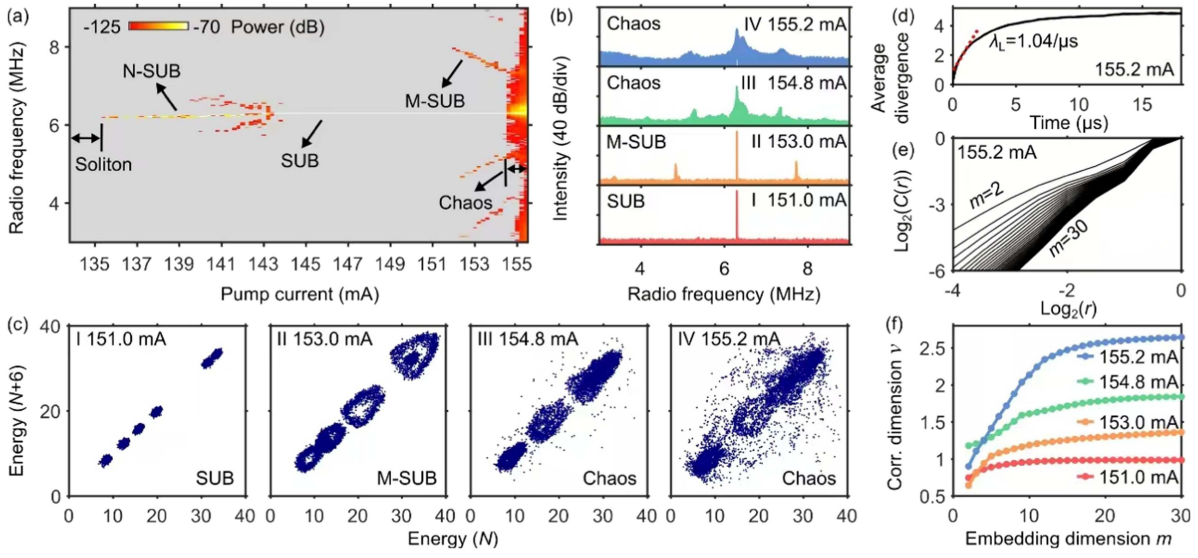

Figure 9. Experimental observation of modulated subharmonic route to chaos. (a) RF spectrum of the laser output as a function of pump current, illustrating successive dynamical transitions from stationary solitons to non-subharmonic (N-SUB), subharmonic (SUB), modulated subharmonic (M-SUB) breathing solitons, and eventually to chaos. The subharmonic breather state is characterized by a rational winding number of $f_b/f_r = 1/6$. (b) Representative spectra corresponding to the SUB (151 mA), M-SUB (153 mA), and chaotic (154.8 and 155.2 mA) states. (c) Corresponding Poincaré sections showing the phase portraits of pulse energy at cavity roundtrip $N + 6$ versus N. (d) Maximum Lyapunov exponent analysis for the chaotic state in (b), IV. The average divergence of nearby trajectories is fitted with $e^{\lambda_L t}$, yielding $\lambda_L = 1.04\ \mu s^{-1}$. (e) Grassberger-Procaccia analysis for the same chaotic state, presenting the correlation integral $C(r)$ versus sphere radius r for different embedding dimensions m. The slope at small r gives an estimate of the correlation dimension. (f) Correlation dimension as a function of embedding dimension for the four dynamical states shown in (b). Adapted from [64].

The Lyapunov characteristic exponent (λ_L) quantifies the rate at which nearby trajectories diverge in phase space; a positive value is a signature of chaos [204,235]. Figure 9(d) shows the exponential divergence of trajectories for the fully chaotic regime, with $\lambda_L = 1.04\ \mu s^{-1}$. We also measured a positive $\lambda_L = 0.399\ \mu s^{-1}$ for the chaotic resonance state, a negative value for the subharmonic state, and a near-zero but still slightly positive $\lambda_L = 0.045\ \mu s^{-1}$ for the modulated subharmonic state, due to measurement noise [64]. To further characterize the system, we estimated the correlation dimension (ν) using the Grassberger-Procaccia algorithm [236]. Figure 9(e) displays the correlation integral $C(r)$ as a function of the sphere radius r for varying embedding dimensions m, showing clear saturation of ν for the chaotic state [Figure 9(c), panel IV], indicative of deterministic chaos. This trend is summarized in Figure 9(f), where all four states exhibit saturated ν values that reflect their increasing dynamical complexity—from periodic to chaotic.

By varying the laser's polarization state (intra-cavity loss), we found that solitons in our laser can also transition to chaos via the subharmonic route—through a subharmonic breather state—previously reported in other physical systems [237,238], and the quasi-periodicity route—through a non-subharmonic breather state—echoing recent observations in magnetic films [224]. As a final remark, we emphasize the critical role of the polarization controller's settings in enabling soliton chaos; merely increasing the pump power from the soliton regime does not typically induce chaotic behavior [64].

6 Conclusions and outlook

We have presented an overview of our recent research demonstrating ultrafast fiber lasers operating in the breathing-soliton regime as a powerful and versatile platform for investigating complex synchronization phenomena and chaotic dynamics relevant to a wide range of physical systems—all within a single nonlinear oscillator, without the need for coupled systems or external forcing. In parallel, we have introduced intelligent control of breather dynamics using GAs, enabling systematic exploration and optimization of dynamic states.

Together, these findings advance our fundamental understanding of nonlinear dynamics and provide a novel experimental framework for probing and controlling complex systems. Notably, we report the first experimental observation of unconventional synchronization structures that had remained unconfirmed in physical systems since the prediction of leaf-like patterns in the circle map model over 25 years ago [200]. We also uncover a modulated subharmonic regime that bridges synchrony and desynchrony, as well as a route to chaos via modulation of subharmonic states—both of which have not been previously observed in physical systems.

The synchronization and desynchronization behaviors observed in breather structures are qualitatively linked to commensurate-incommensurate phase transitions [219], a class of phenomena well known in condensed matter physics. While single-breather oscillations offer a minimal system for studying two-frequency interactions, multi-breather states introduce additional degrees of freedom through their constituent breathing frequencies—paving the way for the investigation of systems with three or more interacting frequencies [214,215,239]. In parallel, since nonlinear interactions among three frequencies are known to give rise to low-dimensional chaos [64,214,215], our results suggest that studying coupled breathing-soliton oscillators and/or multi-breather oscillators could open avenues for exploring high-dimensional chaos (hyperchaos) [240,241] and synchronization of chaos [242,243].

In addition to the ultrafast breathing-soliton lasers discussed, recent studies have extended the breathing-soliton phenomenon to spatiotemporal mode-locked (STML) multimode fiber lasers [244–246]. These systems naturally exhibit complex, high-dimensional nonlinear dynamics, including periodically tunable multimode soliton pulsations [247], spatiotemporal soliton and soliton-molecule behaviors [248,249], and spatiotemporal period-doubling bifurcations [250]. The presence of multiple coupled spatial and temporal modes introduces additional degrees of freedom, possibly enabling interactions among several breathing frequencies and thereby offering a fertile platform for exploring routes to hyperchaos, synchronization and desynchronization of complex oscillatory states, and multi-frequency commensurate-incommensurate transitions. STML fiber lasers thus offer a complementary and more

richly structured setting for extending our studies of breather-mediated nonlinear dynamics. Beyond fiber systems, solid-state lasers have also been shown to support breathing vortex solitons [251], further underscoring the generality of breathing-soliton phenomena across platforms.

Very recently, we have developed a unified model for breather fiber lasers that incorporates the spatiotemporal dynamics of the gain medium. This model reveals the distinct formation mechanisms of breathing solitons under net-normal and near-zero net cavity dispersion, which explain the markedly different experimental behaviors observed in each regime. Specifically, while a combination of Q-switching and soliton shaping is responsible for the formation of breathing solitons under net-normal dispersion, Kerr and dispersion effects dominate the generation of breathing solitons under near-zero dispersion. As partially discussed in this work, these differences manifest in the pump-power range relative to stationary mode-locking, oscillation period, spectral characteristics, and synchronization capabilities. These insights advance our understanding of the physics governing breather dynamics and will be presented in detail in a forthcoming publication [163].

From an applied perspective, our study holds important implications for mastering complex laser behavior, a key requirement for the development of high-performance, turn-key laser sources. Additionally, frequency-locked breather lasers can generate dense RF combs with sub-MHz line spacing—surpassing cavity length limitations—making them highly attractive for high-resolution spectroscopy. Moreover, Arnold tongues provide a robust mechanism for controlling synchronization dynamics. Understanding the conditions that lead to the formation of holes within the synchronization regions is crucial, as this knowledge enables their suppression and ensures stable and reliable system operation. Concurrently, chaotic solitons offer new capabilities for chaos-based technologies such as parallel optical ranging, by leveraging their broad spectral bandwidth, in contrast to microcomb-based systems relying on modulation instability [252,253].

The development of smart, self-optimizing ultrafast fiber oscillators is gaining increasing importance [254,255], as many emerging applications demand lasers with precisely tailored temporal and spectral characteristics. Traditional trial-and-error approaches to laser design and optimization are time-consuming, often irreproducible, and poorly suited for real-time control. Meanwhile, systematic numerical propagation modeling remains computationally expensive, limiting exploration of broader subspaces of useful ultrafast dynamics. Within the broader context of smart ultrafast photonics, artificial intelligence-driven control—particularly through ML approaches—offers a promising path forward. NNs [256,257,144], and especially physics-informed learning frameworks [258], which require less training data and offer greater robustness than purely data-driven models, provide computationally efficient tools for solving both forward and inverse problems in nonlinear systems. These approaches hold strong potential for discovering novel phenomena and deepening our understanding of underlying physical mechanisms. In parallel, advanced signal processing techniques are emerging as powerful tools for analyzing and characterizing the complex radiation dynamics of fiber lasers. One such technique is the inverse scattering transform based on the Zakharov-Shabat system [259]—commonly referred to in optics as the nonlinear Fourier transform—which is applicable in regimes where coherent, localized structures are embedded within dispersive backgrounds [260,106,261]. Additionally, methods such as dynamic mode decomposition and the sparse identification of nonlinear dynamical systems (SINDy) algorithm have shown promise in analyzing the internal dynamics of soliton molecules [262,263] and may be extended to characterize a wide range of periodic and multi-scale nonlinear interactions.

We anticipate that our work will stimulate further research efforts in these directions, both within our group and across the broader ultrafast photonics and nonlinear dynamics communities.

Author contributions

None.

Disclosure statement

The authors declare that they have no competing interests.

Funding information

We acknowledge support from the Innovation Program for Quantum Science and Technology (2023ZD0301000); the National Natural Science Fund of China (12434018, 62475073, 1243000542, 11621404, 11561121003, 11727812, 61775059, 12074122, 62405090, 62035005, 11704123); the Shanghai Natural Science Foundation (23ZR1419000); the China Postdoctoral Science Foundation (2023 M741188, 2024 T170275); the Agence Nationale de la Recherche (ANR–20-CE30–004); the Region Bourgogne-Franche-Comté; the Institut Universitaire de France; and the NATO Science for Peace and Security Program (SPS.MYP.G6137—MELITE).

References

[1] Grelu P, Akhmediev N. Dissipative solitons for mode-locked lasers. Nat Photonics. 2012;6(2):84–92. doi: 10.1038/nphoton.2011.345
[2] Grelu P. Solitary waves in ultrafast fiber lasers: from solitons to dissipative solitons. Opt Commun. 2024;552:130035. doi: 10.1016/j.optcom.2023.130035
[3] Singh P, Senthilnathan K. A review on dissipative optical solitons: a route to photo-bot. Opt Laser Technol. 2025;187:112647. doi: 10.1016/j.optlastec.2025.112647
[4] Soto-Crespo JM, Akhmediev N, Ankiewicz A. Pulsating, creeping, and erupting solitons in dissipative systems. Phys Rev L. 2000;85:2937–2940. doi: 10.1103/PhysRevLett.85.2937
[5] Chang W, Soto-Crespo JM, Vouzas P, et al. Extreme soliton pulsations in dissipative systems. Phys Rev E. 2015;92(2):022926. doi: 10.1103/PhysRevE.92.022926
[6] Peng J, Boscolo S, Zhao Z, et al. Breathing dissipative solitons in mode-locked fiber lasers. Sci Adv. 2019;5(11):eaax1110. doi: 10.1126/sciadv.aax1110
[7] Cundiff ST, Soto-Crespo JM, Akhmediev N. Experimental evidence for soliton explosions. Phys Rev L. 2002;88(7):073903. doi: 10.1103/PhysRevLett.88.073903
[8] Runge AFJ, Broderick NGR, Erkintalo M. Observation of soliton explosions in a passively mode-locked fiber laser. Optica. 2015;2(1):36–39. doi: 10.1364/OPTICA.2.000036
[9] Peng J, Zeng H. Soliton collision induced explosions in a mode-locked fibre laser. Commun Phys. 2019;2:34. doi: 10.1038/s42005-019-0134-8
[10] Liu M, Luo AP, Yan YR, et al. Successive soliton explosions in an ultrafast fiber laser. Opt Lett. 2016;41(6):1181–1184. doi: 10.1364/OL.41.001181
[11] Horowitz M, Barad Y, Silberberg Y. Noiselike pulses with a broadband spectrum generated from an erbium-doped fiber laser. Opt Lett. 1997;22(11):799–801. doi: 10.1364/OL.22.000799
[12] Soto-Crespo JM, Akhmediev N. Soliton as strange attractor: nonlinear synchronization and chaos. Phys Rev L. 2005;95(2):024101. doi: 10.1103/PhysRevLett.95.024101
[13] Lecaplain C, Grelu P, Soto-Crespo J, et al. Dissipative rogue waves generated by chaotic pulse bunching in a mode-locked laser. Phys Rev L. 2012;108(23):233901. doi: 10.1103/PhysRevLett.108.233901
[14] Wu X, Zhang Y, Peng J, et al. Control of spectral extreme events in ultrafast fiber lasers by a genetic algorithm. Laser Photonics Rev. 2023;18(4):2200470. doi: 10.1002/lpor.202200470
[15] Grelu P, Belhache F, Gutty F, et al. Phase-locked soliton pairs in a stretched-pulse fiber laser. Opt Lett. 2002;27(11):966–968. doi: 10.1364/OL.27.000966
[16] Malomed BA. Bound solitons in the nonlinear Schrödinger-ginzburg-landau equation. Phys Rev A. 1991;44(10):6954–6957. doi: 10.1103/PhysRevA.44.6954
[17] Stratmann M, Pagel T, Mitschke F. Experimental observation of temporal soliton molecules. Phys Rev L. 2005;95(14):143902. doi: 10.1103/PhysRevLett.95.143902
[18] Herink G, Kurtz F, Jalali B, et al. Real-time spectral interferometry probes the internal dynamics of femto-second soliton molecules. Sci. 2017;356(6333):50–54. doi: 10.1126/science.aal5326
[19] Krupa K, Nithyanandan K, Andral U, et al. Real-time observation of internal motion within ultrafast dissipative optical soliton molecules. Phys Rev L. 2017;118(24):243901. doi: 10.1103/PhysRevLett.118.243901
[20] Liu X, Yao X, Cui Y. Real-time observation of the buildup of soliton molecules. Phys Rev L. 2018;121(2):023905. doi: 10.1103/PhysRevLett.121.023905
[21] Peng J, Zeng H. Build-up of dissipative optical soliton molecules via diverse soliton interactions. Laser Photonics Rev. 2018;12(8):1800009. doi: 10.1002/lpor.201800009
[22] Wang Z, Nithyanandan K, Coillet A, et al. Optical soliton molecular complexes in a passively mode-locked fibre laser. Nat Commun. 2019;10:830. doi: 10.1038/s41467-019-08755-4
[23] Liu S, Cui Y, Karimi E, et al. On-demand harnessing of photonic soliton molecules. Optica. 2022;9(2):240–250. doi: 10.1364/OPTICA.445704
[24] Zou D, Liu R, Shi Y, et al. Resonantly driven nonlinear dynamics of soliton molecules in ultrafast fiber lasers. Ad Pho. 2025;7(1):016005. doi: 10.1117/1.AP.7.1.016005
[25] Goda K, Jalali B. Dispersive Fourier transformation for fast continuous single-shot measurements. Nat Photonics. 2013;7:102–112. doi: 10.1038/nphoton.2012.359

[26] Mahjoubfar A, Churkin DV, Barland S, et al. Time stretch and its applications. Nat Photonics. 2017;11:341–351. doi: 10.1038/nphoton.2017.76
[27] Wang Y, Wang C, Zhang F, et al. Recent advances in real-time spectrum measurement of soliton dynamics by dispersive Fourier transformation. Rep Prog Phys. 2020;83(11):116401. doi: 10.1088/1361-6633/abbcd7
[28] Godin T, Sader L, Khodadad Kashi A, et al. Recent advances on time-stretch dispersive Fourier transform and its applications. Advances in Physics: X. 2022;7(1):2067487.
[29] Su SW, Gou SC, Liu IK, et al. Oscillons in coupled Bose-Einstein condensates. Phys Rev A. 2015;91(2):023631. doi: 10.1103/PhysRevA.91.023631
[30] Chabchoub A, Hoffmann N, Onorato M, et al. Super rogue waves: observation of a higher-order breather in water waves. Phys Rev . 2012;2(1):011015. doi: 10.1103/PhysRevX.2.011015
[31] Chabchoub A. Tracking breather dynamics in irregular sea state conditions. Phys Rev L. 2016;117(14):144103. doi: 10.1103/PhysRevLett.117.144103
[32] Müller I, Ammelt E, Purwins HG. Self-organized quasiparticles: breathing filaments in a gas discharge system. Phys Rev L. 1999;82(17):3428–3431. doi: 10.1103/PhysRevLett.82.3428
[33] Dudley JM, Genty G, Dias F, et al. Modulation instability, Akhmediev breathers and continuous wave supercontinuum generation. Opt Express. 2009;17(24):21497–21508. doi: 10.1364/OE.17.021497
[34] Kibler B, Fatome J, Finot C, et al. Observation of kuznetsov-Ma soliton dynamics in optical fibre. Sci Rep. 2012;2:463. doi: 10.1038/srep00463
[35] Frisquet B, Kibler B, Millot G. Collision of Akhemediev breathers in nonlinear fiber optics. Phys Rev . 2013;3(4):041032. doi: 10.1103/PhysRevX.3.041032
[36] Toenger S, Godin T, Billet C, et al. Emergent rogue wave structures and statistics in spontaneous modulation instability. Sci Rep. 2015;20:10380. doi: 10.1038/srep10380
[37] Hammani K, Wetzel B, Kibler B, et al. Spectral dynamics of modulation instability described using Akhmediev breather theory. Opt Lett. 2011;36(11):2140–2142. doi: 10.1364/OL.36.002140
[38] Xu G, Gelash A, Chabchoub A, et al. Breather wave molecules. Phys Rev L. 2019;22(8):084101. doi: 10.1103/PhysRevLett.122.084101
[39] Akhmediev NN, Ankiewicz A. Solitons: nonlinear pulses and beams. Optical and Quantum Electronics series. Vol. 5. London, New York: Chapman & Hall; 1997
[40] Copie F, Randoux S, Suret P. The physics of the one-dimensional nonlinear Schrödinger equation in fiber optics: rogue waves, modulation instability and self-foucusing phenomena. Rev Phy. 2020;5:100037. doi: 10.1016/j.revip.2019.100037
[41] Strogatz SH. Nonlinear dynamics and chaos. With Applications to Physics, Biology, Chemistry, and Engineering. 2nd ed. Boca Raton: CRC Press; 2015.
[42] Leo F, Gelens L, Emplit P, et al. Dynamics of one-dimensional Kerr cavity solitons. Opt Express. 2013;21(7):9180–9191. doi: 10.1364/OE.21.009180
[43] Yu M, Jang JK, Okawachi Y, et al. Breather soliton dynamics in microresonators. Nat Commun. 2017;8(7):14569. doi: 10.1038/ncomms14569
[44] Lucas E, Karpov M, Guo H, et al. Breathing dissipative solitons in optical microresonators. Nat Commun. 2017;8:736. doi: 10.1038/s41467-017-00719-w
[45] Cole DC, Papp SB. Subharmonic entrainment of Kerr breather solitons. Phys Rev L. 2019;123(17):173904. doi: 10.1103/PhysRevLett.123.173904
[46] Du Y, Xu Z, Shu X. Spatio-spectral dynamics of the pulsating dissipative solitons in a normal-dispersion fiber laser. OptL. 2018;43(15):3602–3605. doi: 10.1364/OL.43.003602
[47] Xian T, Zhan L, Wang W, et al. Subharmonic entrainment breather solitons in ultrafast lasers. Phys Rev L. 2020;125(16):163901. doi: 10.1103/PhysRevLett.125.163901
[48] Peng J, Zeng H. Experimental observations of breathing dissipative soliton explosions. Phys Rev A. 2019;12:034052. doi: 10.1103/PhysRevApplied.12.034052
[49] Wang X, He J, Mao B, et al. Real-time observation of dissociation dynamics within a pulsating soliton molecule. Opt Express. 2019;27(20):28214–28222. doi: 10.1364/OE.27.028214
[50] Chen HJ, Tan YJ, Long JG, et al. Dynamical diversity of pulsating solitons in a fiber laser. Opt Express. 2019;27(20):28507–28522. doi: 10.1364/OE.27.028507
[51] Luo Y, Xiang Y, Shum PP, et al. Stationary and pulsating vector dissipative solitons in nonlinear multimode interference based fiber laser. Opt Express. 2020;28(3):4216–4224. doi: 10.1364/OE.383305
[52] Liu M, Wei ZW, Li H, et al. Visualizing the "invisible" soliton pulsation in an ultrafast laser. Laser Photonics Rev. 2020;14(4):1900317. doi: 10.1002/lpor.201900317
[53] Wang X, He J, Shi H, et al. Real-time observation of multi-soliton asynchronous pulsations in an L-band dissipative soliton fiber laser. Opt Lett. 2020;45(17):4782–4785. doi: 10.1364/OL.400409
[54] Peng J, Zhao Z, Boscolo S, et al. Breather molecular complexes in a passively mode-locked fiber laser. Laser Photonics Rev. 2021;15(7):2000132. doi: 10.1002/lpor.202000132
[55] Guo J, Cundiff S, Soto-Crespo J, et al. Concurrent passive mode-locked and self-Q-switched operation in laser systems. Phys Rev L. 2021;126(22):224101. doi: 10.1103/PhysRevLett.126.224101

[56] Wu X, Peng J, Boscolo S, et al. Intelligent breathing soliton generation in ultrafast fiber lasers. Laser Photonics Rev. 2022;16(2):2100191. doi: 10.1002/lpor.202100191
[57] Krupa K, Kardaś TM, Stepanenko Y. Real-time observation of double-Hopf bifurcation in an ultrafast all-PM fiber laser. Laser Photonics Rev. 2022;16(10):2100646. doi: 10.1002/lpor.202100646
[58] Du Y, He Z, Gao Q, et al. Synchronous and asynchronous pulsating dual solitons in lasers. Opt L. 2022;47(13):3323–3326. doi: 10.1364/OL.461461
[59] Zhou Y, Ren YX, Shi J, et al. Breathing dissipative soliton molecule switching in a bidirectional mode-locked fiber laser. Advanced Photonics Research. 2022;3(4):2100318. doi: 10.1002/adpr.202100318
[60] Wu X, Peng J, Boscolo S, et al. Synchronization, desynchronization, and intermediate regime of breathing solitons and soliton molecules in a laser cavity. Phys Rev L. 2023;131(26):263802. doi: 10.1103/PhysRevLett.131.263802
[61] Wang Z, Coillet A, Hamdi S, et al. Spectral pulsations of dissipative solitons in ultrafast fiber lasers: period doubling and beyond. Laser Photonics Rev. 2023;17(3):2200298. doi: 10.1002/lpor.202200298
[62] Lu M, Wang X, Li K, et al. Transient behaviors of the pulsating dissipative solitons in a net normal-dispersion fiber laser. La Phy. 2023;33(1):015101. doi: 10.1088/1555-6611/aca756
[63] Cui Y, Zhang Y, Huang L, et al. Dichromatic "breather molecules" in a mode-locked fiber laser. Phys Rev L. 2023;130(15):153801. doi: 10.1103/PhysRevLett.130.153801
[64] Kang H, Zhou A, Zhang Y, et al. Observation of optical chaotic solitons and modulated subharmonic route to chaos in mode-locked laser. Phys Rev L. 2024;133(26):263801. doi: 10.1103/PhysRevLett.133.263801
[65] Fan Y, Wang X, Fu M, et al. Dynamic diversity of asynchronous pulsating solitons in fiber lasers. Opt Laser Technol. 2024;176:110931. doi: 10.1016/j.optlastec.2024.110931
[66] Li Y, Xia R, Liu J, et al. Real-time measurements of breathing dissipative soliton pairs in mode-locked fiber lasers. Opt Laser Technol. 2024;175:110900. doi: 10.1016/j.optlastec.2024.110900
[67] Wang G, Fu B, Sun J, et al. Bridging the mode-locked and Q-switched regimes in fiber lasers. Laser Photonics Rev. 2025;19:2402171. doi: 10.1002/lpor.202402171
[68] Wu X, Peng J, Yuan B, et al. Unveiling the complexity of Arnold's tongues in a breathing-soliton laser. Sci Adv. 2025;11(12):eads3660. doi: 10.1126/sciadv.ads3660
[69] Wu X, Zhang Y, Peng J, et al. Farey tree and devil's staircase of frequency-locked breathers in ultrafast lasers. Nat Commun. 2022;13(1):5784. doi: 10.1038/s41467-022-33525-0
[70] Du W, Li H, Li J, et al. Vector dynamics of pulsating solitons in an ultrafast fiber laser. Opt Lett. 2020;45(18):5024–5027. doi: 10.1364/OL.400001
[71] Li TJ, Liu M, Luo AP, et al. Vector features of pulsating soliton in an ultrafast fiber laser. Opt Express. 2020;28(21):32010–32018. doi: 10.1364/OE.404674
[72] Wang Z, Li H, Li J, et al. Generation and vector features of pulsating dissipative-soliton-resonance pulses in a figure-of-eight fiber laser. Opt Laser Technol. 2023;161:109132. doi: 10.1016/j.optlastec.2023.109132
[73] Huang Z, Sergeyev S, Wang Q, et al. Dissipative soliton breathing dynamics driven by desynchronization of orthogonal polarization states. Advanced Photonics Nexus. 2023;2(6):066007. doi: 10.1117/1.APN.2.6.066007
[74] Deng D, Zhang H, Zu J, et al. Buildup dynamics of a pulsating dissipative soliton in an all-normal-dispersion PM Yb-doped fiber laser with a NALM. Opt L. 2021;46(7):1612–1615. doi: 10.1364/OL.421697
[75] Yuan B, Peng J, Kang H, et al. The devil's staircase in a figure-of-nine laser. Opt Laser Technol. 2025;191:113310. doi: 10.1016/j.optlastec.2025.113310
[76] Akosman AE, Sander MY. Route towards extreme optical pulsation in linear cavity ultrafast fibre lasers. Sci Rep. 2018;8(1):13385. doi: 10.1038/s41598-018-31725-7
[77] Cao B, Zhao K, Gao C, et al. Observation of pulsating dissipative solitons in a Mamyshev oscillator. Phys Rev A. 2022;106(2):023519. doi: 10.1103/PhysRevA.106.023519
[78] Suzuki M, Boyraz O, Asghari H, et al. Spectral periodicity in soliton explosions on a broadband mode-locked Yb fiber laser using time-stretch spectroscopy. Opt Lett. 2018;43(8):1862–1865. doi: 10.1364/OL.43.001862
[79] Qi JJ, Liu M, Li TJ, et al. Periodic transition between two evolving soliton pulsation states in an Yb-doped fiber laser. Opt Express. 2023;31(4):7023–7031. doi: 10.1364/OE.484204
[80] Fu M, Wang X, Fan Y, et al. Real-time observation of soliton pulsation and explosion in an Yb-doped fiber laser. Laser Phys. 2024;34(5):055102. doi: 10.1088/1555-6611/ad38b0
[81] Li J, Li H, Wang Z, et al. Real-time observation of pulsating solitons with central wavelength oscillation in an ultrafast fiber laser. Opt Laser Technol. 2022;155:108429. doi: 10.1016/j.optlastec.2022.108429
[82] Ji Y, Yang Y, Song Y, et al. Dynamics of pulsating solitons with chaotic behaviors from a 1.7 μm ultrafast fiber laser. Chaos, Solitons Fractals. 2024;187:115379. doi: 10.1016/j.chaos.2024.115379
[83] Wang P, Xiao X, Grelu P. Subsideband generation associated with period-N pulsations in Tm soliton fiber lasers. IEEE Pho J. 2017;9(4):1–8. doi: 10.1109/JPHOT.2017.2733044
[84] Liu J, Li M, He J, et al. Noisy soliton pulsation and its dynamics in a mid-infrared ultrafast fiber laser. Chaos, Solitons Fractals. 2023;177:114199. doi: 10.1016/j.chaos.2023.114199
[85] Zhou Y, Ren YX, Shi J, et al. Dynamics of breathing dissipative soliton pairs in a bidirectional ultrafast fiber laser. Opt Lett. 2022;47(8):1968–1971. doi: 10.1364/OL.454658

[86] Soto-Crespo JM, Grapinet M, Grelu P, et al. Bifurcations and multiple-period soliton pulsations in a passively mode-locked fiber laser. Phys Rev E. 2004;70:066612. doi: 10.1103/PhysRevE.70.066612
[87] Haus HA. Mode-locking of lasers. IEEE J Sel Top Quantum Electron. 2000;6(6):1173–1185.
[88] Wang Z, Wang Z, Liu Y, et al. Self-organized compound pattern and pulsation of dissipative solitons in a passively mode-locked fiber laser. Opt Lett. 2018;43(3):478–481. doi: 10.1364/OL.43.000478
[89] He Z, Du Y, Zeng C, et al. Soliton metamorphosis dynamics in ultrafast fiber lasers. Phys Rev A. 2021;103:053516. doi: 10.1103/PhysRevA.103.053516
[90] Yuan Z, Luo S, Dai K, et al. Transient breathing dynamics of dissipative soliton in an ultrafast laser. Opt Laser Technol. 2024;176:111051. doi: 10.1016/j.optlastec.2024.111051
[91] Matsas VJ, Newson TP, Richardson DJ, et al. Selfstarting passively mode-locked fibre ring soliton laser exploiting nonlinear polarisation rotation. Electron Lett. 1992;28(15):1391–1393. doi: 10.1049/el:19920885
[92] Lapre C, Meng F, Hary M, et al. Genetic algorithm optimization of broadband operation in a noise-like pulse fiber laser. Sci Rep. 2023;13(1):1865. doi: 10.1038/s41598-023-28689-8
[93] Zheng PZ, Li TJ, Xia HD, et al. Autosetting soliton pulsation in a fiber laser by an improved depth-first search algorithm. Opt Express. 2021;29(21):34684–34694. doi: 10.1364/OE.438605
[94] Hellwig T, Walbaum T, Gross P, et al. Automated characterization and alignment of passively mode-locked fiber lasers based on nonlinear polarization rotation. Appl Phys B. 2010;101(3):565–570. doi: 10.1007/s00340-010-4224-2
[95] Shen X, Li W, Yan M, et al. Electronic control of nonlinear-polarization-rotation mode locking in Yb-doped fiber lasers. Opt Lett. 2012;37(16):3426–3428. doi: 10.1364/OL.37.003426
[96] Radnatarov D, Khripunov S, Kobtsev S, et al. Automatic electronic-controlled mode locking self-start in fibre lasers with non-linear polarisation evolution. Opt Express. 2013;21(18):20626–20631. doi: 10.1364/OE.21.020626
[97] Winters DG, Kirchner MS, Backus SJ, et al. Electronic initiation and optimization of nonlinear polarization evolution mode-locking in a fiber laser. Opt Express. 2017;25(26):33216–33225. doi: 10.1364/OE.25.033216
[98] Huang Q, Huang Z, Mou C. Transient soliton dynamics in a mode-locked fiber laser: From stationary to pulsation. Opt Lett. 2021;46(22):5683–5686. doi: 10.1364/OL.442740
[99] Sucha G, Bolton RS, Weiss S, et al. Period doubling and quasi-periodicity in additive-pulse mode-locked lasers. Opt Lett. 1995;20(17):1794–1796. doi: 10.1364/OL.20.001794
[100] Xing Q, Chai L, Zhang W, et al. Regular, period-doubling, quasi-periodic, and chaotic behavior in a self-mode-locked Ti: sapphire laser. Opt Commun. 1999;162(1-3):71–74. doi: 10.1016/S0030-4018(99)00077-2
[101] Fernandez A, Fuji T, Poppe A, et al. Chirped-pulse oscillators: A route to high-power femtosecond pulses without external amplification. Opt Lett. 2004;29(12):1366–1368. doi: 10.1364/OL.29.001366
[102] Zhao LM, Tang DY, Lin F, et al. Observation of period-doubling bifurcations in a femtosecond fiber soliton laser with dispersion management cavity. Opt Express. 2004;12(19):4573–4578. doi: 10.1364/OPEX.12.004573
[103] Zhao LM, Tang DY, Cheng TH, et al. Period-doubling of dispersion-managed solitons in an Erbium-doped fiber laser at around zero dispersion. Opt Commun. 2007;278(2):428–433. doi: 10.1016/j.optcom.2007.06.024
[104] Sugavanam S, Tarasov N, Churkin D. Real-time intensity domain characterization of fibre lasers using spatio-temporal dynamics. Applied Sciences. 2016;6:64. doi: 10.3390/app6030065
[105] Jannson T. Real-time fourier transformation in dispersive optical fibers. OptL. 1983;8(4):232–234. doi: 10.1364/OL.8.000232
[106] Ryczkowski P, Närhi M, Billet C, et al. Real-time full-field characterization of transient dissipative soliton dynamics in a mode-locked laser. Nat Photonics. 2018;12(4):221–227. doi: 10.1038/s41566-018-0106-7
[107] Herink G, Jalali B, Ropers C, et al. Resolving the build-up of femtosecond mode-locking with single-shot spectroscopy at 90 MHz frame rate. Nat Photonics. 2016;10(5):321–326. doi: 10.1038/nphoton.2016.38
[108] Lapre C, Billet C, Meng F, et al. Real-time characterization of spectral instabilities in a mode-locked fibre laser exhibiting soliton-similariton dynamics. Sci Rep. 2019;9(1):13950. doi: 10.1038/s41598-019-50022-5
[109] Wei X, Li B, Yu Y, et al. Unveiling multi-scale laser dynamics through time-stretch and time-lens spectroscopies. Opt Express. 2017;25(23):29098–29120. doi: 10.1364/OE.25.029098
[110] Zhang Y, Cui Y, Huang L, et al. Full-field real-time characterization of creeping solitons dynamics in a mode-locked fiber laser. Opt L. 2020;45(22):6246–6249. doi: 10.1364/OL.404778
[111] Lu M, Wang X, Li K, et al. Spectral pulsations of evolving soliton molecules in an anomalous dispersion fiber laser. Laser Phys Lett. 2023;20(5):055102. doi: 10.1088/1612-202X/accdd3
[112] Chen H, Guo J, Liang W, et al. Dynamical diversity of FWM-induced pulsating solitons in an ultrafast fiber laser. Sci Rep. 2025;15(1):11280. doi: 10.1038/s41598-025-94930-1
[113] Li Y, Xia R, Liu J, et al. Transient multi-pulse dynamics involving breathing and explosion in mode-locked fiber lasers. Opt Commun. 2025;577:131409. doi: 10.1016/j.optcom.2024.131409
[114] Xu H, Lin W, Hu X, et al. Real-time birth-to-annihilation dynamics of dissipative kerr cavity soliton. Ch Opt L. 2024;22(11):111903. doi: 10.3788/COL202422.111903
[115] Zhang H, Du Y, Zeng C, et al. The dissipative talbot soliton fiber laser. Sci Adv. 2024;10(11):eadl2125. doi: 10.1126/sciadv.adl2125

[116] Chang Z, Xian T, Hao C, et al. Synchronization of breathing-soliton and dispersive wave in mode-locked fiber lasers. IEEE Photonics Technol Lett. 2025;37(7):381–384. doi: 10.1109/LPT.2025.3547784
[117] Han Y, Gao B, Hao Y, et al. Paths from stationary to chaos in passively mode-locked fiber lasers: research progress of soliton pulsations and soliton explosions. J Phys B: At Mol Opt Phys. 2022;55(22):222001. doi: 10.1088/1361-6455/ac9204
[118] Chen J, Zhao X, Li T, et al. Generation and observation of ultrafast spectro-temporal dynamics of different pulsating solitons from a fiber laser. Opt Express. 2020;28(9):14127–14133. doi: 10.1364/OE.392616
[119] Du Y, Zeng C, He Z, et al. Trampolinelike pulsating soliton fiber lasers. Phys Rev A. 2021;104:023503. doi: 10.1103/PhysRevA.104.023503
[120] Mao D, Yuan Z, Dai K, et al. Temporal and spatiotemporal soliton molecules in ultrafast fibre lasers. Nanop. 2025;14(6):677–706. doi: 10.1515/nanoph-2024-0590
[121] Shen H, Zhou R, Li Y, et al. Directly gain control of loosely bound pulsating soliton pairs in a mode-locked fiber laser. Opt Express. 2025;33(8):18454–18466. doi: 10.1364/OE.558670
[122] Hou L, Hou Y, Liu Y, et al. Breathers in mode-locked lasers based on saturable absorbers. AcPSn. 2025;74(4):044206. doi: 10.7498/aps.74.20241505
[123] Han Y, Gao B, Wu G, et al. Analysis of various soliton pulsation spectro-temporal dynamics in anomalous dispersion fiber laser. Opt Laser Technol. 2022;148:107690. doi: 10.1016/j.optlastec.2021.107690
[124] Boscolo S, Peng J, Finot C. Design and applications of in-cavity pulse shaping by spectral sculpturing in mode-locked fibre lasers. Applied Sciences. 2015;5(4):1379–1398. doi: 10.3390/app5041379
[125] Yue L, Xue F, Wei Z, et al. An experiment of dynamical behaviours in an erbium-doped fibre-ring laser with loss modulation. Chin Phys B. 2009;18(8):3318–3324. doi: 10.1088/1674-1056/18/8/036
[126] Liu Y, Zhang W, Feng X. Frequency locking, quasiperiodicity, and chaos in dual-frequency loss-modulated erbium-doped fiber lasers. Chin. Opt. Lett. 2009;7(8):699–702. doi: 10.3788/COL20090708.0699
[127] Zou D, Song Y, Gat O, et al. Synchronization of the internal dynamics of optical soliton molecules. Optica. 2022;9(11):1307–1313. doi: 10.1364/OPTICA.473819
[128] Feng J, Zhang Z, Wei J, et al. Active breathing pulses induced by the periodic loss in a passive mode-locked laser. Opt Lett. 2025;50(7):2326–2329. doi: 10.1364/OL.554512
[129] Hoang VT, Boussafa Y, Sader L, et al. Optimizing supercontinuum spectro-temporal properties by leveraging machine learning towards multi-photon microscopy. Frontiers in Photonics. 2022;3, doi: 10.3389/fphot.2022.940902
[130] Hary M, Salmela L, Ryczkowski P, et al. Tailored supercontinuum generation using genetic algorithm optimized Fourier domain pulse shaping. Opt Lett. 2023;48(17):4512–4515. doi: 10.1364/OL.492064
[131] Andral U, Buguet J, Si Fodil R, et al. Toward an autosetting mode-locked fiber laser cavity. J Opt Soc Am B. 2016;33(5):825–833. doi: 10.1364/JOSAB.33.000825
[132] Woodward RI, Kelleher EJR. Towards 'smart lasers': self-optimisation of an ultrafast pulse source using a genetic algorithm. Sci Rep. 2016;6(1):37616. doi: 10.1038/srep37616
[133] Han D, Guo R, Li G, et al. Automatic mode-locked fiber laser based on adaptive genetic algorithm. Opt Fiber Technol. 2024;83:103677. doi: 10.1016/j.yofte.2024.103677
[134] Girardot J, Coillet A, Nafa M, et al. On-demand generation of soliton molecules through evolutionary algorithm optimization. Opt Lett. 2022;47(1):134–137. doi: 10.1364/OL.446075
[135] Pu G, Yi L, Zhang L, et al. Intelligent programmable mode-locked fiber laser with a human-like algorithm. Optica. 2019;6(3):362–369. doi: 10.1364/OPTICA.6.000362
[136] Holland JH. Genetic algorithms. Sci Am. 1992;267(1):66–73. doi: 10.1038/scientificamerican0792-66
[137] Mitchell M. An Introduction to Genetic Algorithms. MIT press; 1998.
[138] Wu X, Peng J, Zhang Y, et al. Principles and research advances of intelligent mode-locked fiber lasers. Chin J Lasers . 2023;50(11):1101006.
[139] Sun C, Kaiser E, Brunton SL, et al. Deep reinforcement learning for optical systems: a case study of mode-locked lasers. MLST. 2020;1(4):045013.
[140] Liu H, Sun C, Zhang H. Comprehensive exploration: automatic mode-locking technology and its multi-disciplinary applications. Infrared Physics Technology. 2024;138:105247. doi: 10.1016/j.infrared.2024.105247
[141] Di Lauro L, Sciara S, Fischer B, et al. Optimization methods for integrated and programmable photonics in next-generation classical and quantum smart communication and signal processing systems. Adv Opt Photonics. 2025;17(3):526–622. doi: 10.1364/AOP.533504
[142] Han X, Huang Z, Yue J, et al. Optimizing ultrashort pulse in fiber laser based on artificial intelligence algorithm. Sci Rep. 2024;14(1):7919. doi: 10.1038/s41598-024-58630-6
[143] Zhang C, Xiang P, Zhu W, et al. Intelligent controllable ultrafast fiber laser via deep learning and adaptive optimization algorithm. Infrared Physics Technology. 2024;142:105572. doi: 10.1016/j.infrared.2024.105572
[144] Pu G, Liu R, Yang H, et al. Fast predicting the complex nonlinear dynamics of mode-locked fiber laser by a recurrent neural network with prior information feeding. Laser Photonics Rev. 2023;17(6):2200363. doi: 10.1002/lpor.202200363
[145] Si ZZ, Wang DL, Zhu BW, et al. Deep learning for dynamic modeling and coded information storage of vector-soliton pulsations in mode-locked fiber lasers. Laser Photonics Rev. 2024;18(12):2400097. doi: 10.1002/lpor.202400097

[146] Zhang B, Han D, Li T, et al. Deep learning method for predicting the complex nonlinear dynamics of passively mode-locked fiber laser. Opt Commun. 2025;575:131286. doi: 10.1016/j.optcom.2024.131286
[147] Haus HA. Theory of mode locking with a fast saturable absorber. J Appl Phys. 1975;46(7):3049–3058. doi: 10.1063/1.321997
[148] Akhmediev N, Soto-Crespo JM, Town G. Pulsating solitons, chaotic solitons, period doubling, and pulse coexistence in mode-locked lasers: complex Ginzburg-Landau equation approach. Physical Review E. 2001;63:056602. doi: 10.1103/PhysRevE.63.056602
[149] Tsoy EN, Akhmediev N. Bifurcations from stationary to pulsating solitons in the cubic-quintic complex Ginzburg-Landau equation. Phys Lett A. 2005;343(6):417–422. doi: 10.1016/j.physleta.2005.05.102
[150] Song L, Li L, Li Z, et al. Effect of third-order dispersion on pulsating, erupting and creeping solitons. Opt Commun. 2005;249(1):301–309. doi: 10.1016/j.optcom.2005.01.015
[151] Uzunov IM, Georgiev ZD, Arabadzhiev TN. Transitions of stationary to pulsating solutions in the complex cubic-quintic Ginzburg-Landau equation under the influence of nonlinear gain and higher-order effects. Phys Rev E. 2018;97:052215. doi: 10.1103/PhysRevE.97.052215
[152] He R, Wang Z, Liu Y, et al. Dynamic evolution of pulsating solitons in a dissipative system with the gain saturation effect. Opt Express. 2018;26(25):33116–33128. doi: 10.1364/OE.26.033116
[153] Nana L, Kuetche Saadeu G. Impact of higher-order effects on the stationary and pulsating localized soliton in a nonlinear and dissipative medium. Chaos, Solitons Fractals. 2023;173:113671. doi: 10.1016/j.chaos.2023.113671
[154] Li Z, He J, Wang S, et al. Synchronization and transition dynamics between external modulation and pulsating solitons. J Light Technol. 2025;43(17):8429–8434. doi: 10.1109/JLT.2025.3587941
[155] Ferreira MFS. Variational approach to stationary and pulsating dissipative optical solitons. IET Optelectron. 2018;12(3):122–125. doi: 10.1049/iet-opt.2017.0121
[156] Agrawal GP. Nonlinear Fiber Optics. 6th ed. San Francisco, CA: Academic Press; 2019.
[157] Yang S, Zhu Z, Qi Y, et al. Internal motion within pulsating pure-quartic soliton molecules in a fiber laser. Chaos, Solitons Fractals. 2023;172:113544. doi: 10.1016/j.chaos.2023.113544
[158] Luo M, Zhang ZX, Jin JH, et al. Pure high-even-order dispersion pulsating dynamics in soliton fiber lasers. Chaos, Solitons Fractals. 2025;192:115967. doi: 10.1016/j.chaos.2024.115967
[159] Wu ZL, Zhang ZX, Li TJ, et al. Pulsating dynamics of dissipative pure-quartic soliton in a fiber laser. Opt Express. 2025;33(5):10129–10139. doi: 10.1364/OE.555042
[160] Wang Z, Lin Y, Song Y, et al. Revealing the dynamics of multiple solitons and soliton pulsations in a quartic-dispersion fiber laser. Laser Photonics Rev. 2025;e01851.
[161] Huygens C. Œuvres Complètes. de Christiaan Huygens. Vol. 5. The Netherlands: The Hague: Martinus Nijhof; 1893.
[162] Pikovsky A, Rosenblum M, Kurths J. Synchronization: A Universal Concept in Nonlinear Science. Cambridge, UK: Cambridge University Press; 2001.
[163] Y Z, Yuan B, & Wu X, et al. A unified model for breathing solitons in fibre lasers: Mechanisms across below- and above-threshold regimes. Submitted. 2025.
[164] Grüner G. The dynamics of charge-density waves. Rev Mod Phys. 1988;60(4):1129–1181. doi: 10.1103/RevModPhys.60.1129
[165] Shapiro S. Josephson currents in superconducting tunneling: the effect of microwaves and other observations. Phys Rev L. 1963;11(2):80–82. doi: 10.1103/PhysRevLett.11.80
[166] Van der Pol B, Van der Mark J. Frequency demultiplication. Nature. 1927;120:363–364. doi: 10.1038/120363a0
[167] Zhang J, Hess PW, Kyprianidis A, et al. Observation of a discrete time crystal. Nature. 2017;543(7644):217–220. doi: 10.1038/nature21413
[168] Jensen MH, Bak P, Bohr T. Complete devil's staircase, fractal dimension, and universality of mode-locking structure in the circle map. Phys Rev L. 1983;50(21):1637–1639. doi: 10.1103/PhysRevLett.50.1637
[169] Bak P. Devil's staircase. Phys Today. 1986;39(12):38–45. doi: 10.1063/1.881047
[170] Bak P, von Boehm J. Ising model with solitons, phasons, and "the devil's staircase. Physical Reviews B. 1980;21(11):5297–5308. doi: 10.1103/PhysRevB.21.5297
[171] Brown SE, Mozurkewich G, Grüner G. Subharmonic Shapiro steps and devil's-staircase behavior in driven charge-density-wave systems. Phys Rev L. 1984;52(25):2277–2280. doi: 10.1103/PhysRevLett.52.2277
[172] Jin FF, Neelin JD, Ghil M. El Niño on the devil's staircase: annual subharmonic steps to chaos. Sci. 1994;264(5155):70–72. doi: 10.1126/science.264.5155.70
[173] Kuroda K, Arai Y, Rezaei. Nea. Devil's staircase transition of the electronic structures in CeSb. Nat Commun. 2020;11:2888. doi: 10.1038/s41467-020-16707-6
[174] Winful H, Chen Y, Liu J. Frequency locking, quasiperiodicity, and chaos in modulated self-pulsing semiconductor lasers. Appl Phys L. 1986;48:616–618. doi: 10.1063/1.96771
[175] Baums D, Elsässer W, Göbel EO. Farey tree and devil's staircase of a modulated external-cavity semiconductor laser. Phys Rev L. 1989;63(2):155–158. doi: 10.1103/PhysRevLett.63.155
[176] Wünsche HJ, Bauer S, Kreissl J, et al. Synchronization of delay-coupled oscillators: a study of semiconductor lasers. Phys Rev L. 2005;94(16):163901. doi: 10.1103/PhysRevLett.94.163901

[177] Shortiss K, Lingnau B, Dubois F, et al. Harmonic frequency locking and tuning of comb frequency spacing through optical injection. Opt Express. 2019;27(25):36976–36989. doi: 10.1364/OE.27.036976
[178] Greilich A, Kopteva NE, Korenev VL, et al. Exploring nonlinear dynamics in periodically driven time crystal from synchronization to chaotic motion. Nat Commun. 2025;16(1):2936. doi: 10.1038/s41467-025-58400-6
[179] Jang JK, Klenner A, Ji X, et al. Synchronization of coupled optical microresonators. Nat Photonics. 2018;12:688–693. doi: 10.1038/s41566-018-0261-x
[180] Xu Y, Lin Y, Nielsen A, et al. Harmonic and rational harmonic driving of microresonator soliton frequency combs. Optic. 2020;7:940–946. doi: 10.1364/OPTICA.392571
[181] Thévenin J, Romanelli M, Vallet M, et al. Resonance assisted synchronization of coupled oscillators: frequency locking without phase locking. Phys Rev L. 2011;107(10):104101. doi: 10.1103/PhysRevLett.107.104101
[182] Otsuka K, Hwong SL, Nguyen BA. Intrinsic instability and locking of pulsation frequencies in free-running two-mode class-B lasers. Phys Rev A. 2000;61(5):053815. doi: 10.1103/PhysRevA.61.053815
[183] Kurtz F, Ropers C, Herink G. Resonant excitation and all-optical switching of femtosecond soliton molecules. Nat Photonics. 2020;14:9–13. doi: 10.1038/s41566-019-0530-3
[184] Hentschel HGE, Procaccia I. The infinite number of generalized dimensions of fractals and strange attractors. Physica D. 1983;8(3):435–444. doi: 10.1016/0167-2789(83)90235-X
[185] Zhang Y, Wu X, Peng J, et al. On the universality of fractal breathers in mode-locked fibre lasers. Opt Commun. 2023;547:129845. doi: 10.1016/j.optcom.2023.129845
[186] Ni Y, Xie Z, Sheng Y, et al. Revealing fractal dynamics by dispersion tuning in a mode-locked fiber laser. J Opt Soc Am B. 2024;41(10):2285–2289. doi: 10.1364/JOSAB.533973
[187] Dong H, Yao X, Zhang Q. Phase-locking characteristics and dynamics of the subharmonic entrainment of breathing temporal solitons. Chaos. 2025;35(2):023152. doi: 10.1063/5.0229600
[188] Liu G, Ma X, Zhou K, et al. Farey tree locking of terahertz quantum cascade laser frequency combs. Light: Sci Appl. 2025;14(1):147. doi: 10.1038/s41377-025-01819-9
[189] Adler R. A study of locking phenomena in oscillators. Proc IRE. 1946;34(6):351–357.
[190] Arnold VI. Mathematical Methods of Classical Mechanics. 1sted. New York, Heidelberg, Berlin: Springer-Verlag; 1978.
[191] Shim SB, Imboden M, Mohanty P. Synchronized oscillation in coupled nanomechanical oscillators. Sci. 2007;316(5821):95–99. doi: 10.1126/science.1137307
[192] Kim BY, Jang JK, Okawachi Y, et al. Synchronization of nonsolitonic Kerr combs. Sci Adv. 2021;7(43):eabi4362. doi: 10.1126/sciadv.abi4362
[193] Skryabin D, Fan Z, Villois A, et al. Threshold of complexity and Arnold tongues in kerr-ring microresonators. Phys Rev A. 2021;103(1):L011502. doi: 10.1103/PhysRevA.103.L011502
[194] Droin C, Paquet ER, Naef F. Low-dimensional dynamics of two coupled biological oscillators. Nat Phys. 2019;15:1086–1094. doi: 10.1038/s41567-019-0598-1
[195] Font-Muñoz JS, Sourisseau M, Cohen-Sánchez A, et al. Pelagic diatoms communicate through synchronized beacon natural fluorescence signaling. Sci Adv. 2021;7(51):eabj5230. doi: 10.1126/sciadv.abj5230
[196] Rodrigues CC, Kersul CM, Primo AG, et al. Optomechanical synchronization across multi-octave frequency spans. Nat Commun. 2021;12:5625. doi: 10.1038/s41467-021-25884-x
[197] Laskar AW, Adhikary P, Mondal S, et al. Observation of quantum phase synchronization in spin-1 atoms. Phys Rev L. 2020;125(1):013601. doi: 10.1103/PhysRevLett.125.013601
[198] Zheng E, Brandenbourger M, Robinet L, et al. Self-oscillation and synchronization transitions in elastoactive structures. Phys Rev L. 2023;130(17):178202. doi: 10.1103/PhysRevLett.130.178202
[199] Reichhardt C, Nori F. Phase locking, devil's staircases, Farey trees, and Arnold tongues in driven vortex lattices with periodic pinning. Phys Rev L. 1999;82(2):414–417. doi: 10.1103/PhysRevLett.82.414
[200] Feudel U, Grebogi C, Ott E. Phase-locking in quasiperiodically forced systems. Phys Rep. 1997;290(1–2):11–25. doi: 10.1016/S0370-1573(97)00055-0
[201] Papaioannou GV, Yue DK, Triantafyllou MS, et al. Evidence of holes in the Arnold tongues of flow past two oscillating cylinders. Phys Rev L. 2006;96(1):014501. doi: 10.1103/PhysRevLett.96.014501
[202] Turing AM. The chemical basis of morphogenesis. Philosophical Transactions of the Royal Society of London. Series B, Biological Sciences.. Vol. 237. London, UK: The Royal Society; 1952. p. 37–72.
[203] Saxena G, Prasad A, Ramaswamy R. Amplitude death: the emergence of stationarity in coupled nonlinear systems. Phys Rep. 2012;521(5):205–228. doi: 10.1016/j.physrep.2012.09.003
[204] Ott E. Chaos in Dynamical Systems. 2nd ed. Cambridge, England: Cambridge University Press; 2002.
[205] Bergé P, Pomeau Y, Vidal C. Order within Chaos: Towards a Deterministic Approach to Turbulence. Wiley-VCH; 1987.
[206] Moille G, Sridhar SK, Shandilya P, et al. Toward chaotic group velocity hopping of an on-chip dissipative Kerr soliton. Phys Rev L. 2025;13:133802. doi: 10.1103/2k7d-p7rm
[207] Haboucha A, Leblond H, Salhi M, et al. Analysis of soliton pattern formation in passively mode-locked fiber lasers. Phys Rev A. 2008;78(4):043806. doi: 10.1103/PhysRevA.78.043806
[208] Cole DC, Lamb ES, Del'Haye P, et al. Soliton crystals in Kerr resonators. Nat Photonics. 2017;11:671–676. doi: 10.1038/s41566-017-0009-z

[209] Karpov M, Pfeiffer MHP, Guo H, et al. Dynamics of soliton crystals in optical microresonators. Nat Phys. 2019;15:1071–1077.doi: 10.1038/s41567-019-0635-0
[210] Lu Z, Chen HJ, Wang W, et al. Synthesized soliton crystals. Nat Commun. 2021;12:3179. doi: 10.1038/s41467-021-23172-2
[211] He W, Pang M, Yeh DH, et al. Formation of optical supramolecular structures in a fibre laser by tailoring long-range soliton interactions. Nat Commun. 2019;10:5756. doi: 10.1038/s41467-019-13746-6
[212] Turaev D, Vladimirov AG, Zelik S. Long-range interaction and synchronization of oscillating dissipative solitons. Phys Rev L. 2012;108(26):263906. doi: 10.1103/PhysRevLett.108.263906
[213] Du Y, Han M, Cheng P, et al. Pulsating soliton with broadened Kelly sidebands in an ultrafast fiber laser. Opt L. 2019;44(16):4087–4090. doi: 10.1364/OL.44.004087
[214] Grebogi C, Ott E, Yorke JA. Are three-frequency quasiperiodic orbits to be expected in typical nonlinear dynamical systems? Phys Rev L. 1983;51(5):339–342. doi: 10.1103/PhysRevLett.51.339
[215] Cumming A, Linsay PS. Quasiperiodicity and chaos in a system with three competing frequencies. Phys Rev L. 1988;60(26):2719–2722. doi: 10.1103/PhysRevLett.60.2719
[216] Rosenblum MG, Pikovsky AS, Kurths J. From phase to lag synchronization in coupled chaotic oscillators. Phys Rev L. 1997;78(22):4193–4196. doi: 10.1103/PhysRevLett.78.4193
[217] Taherion S, Lai YC. Observability of lag synchronization of coupled chaotic oscillators. Phys Rev E. 1999;59(6):R6247–R6250. doi: 10.1103/PhysRevE.59.R6247
[218] Amrani F, Haboucha A, Salhi M, et al. Dissipative solitons compounds in a fiber laser. analogy with the states of the matter. Appl Phys B. 2010;99:107–114. doi: 10.1007/s00340-009-3774-7
[219] Bak P. Commensurate phases, incommensurate phases and the devil's staircase. Rep Prog Phys. 1982;45(6):587–629. doi: 10.1088/0034-4885/45/6/001
[220] Eilbeck JC, Lomdahl PS, Newell AC. Chaos in the inhomogeneously driven sine-Gordon equation. Phys Lett A. 1981;87(1–2):1–4. doi: 10.1016/0375-9601(81)90599-5
[221] Nozaki K, Bekki N. Chaos in a perturbed nonlinear Schrödinger equation. Phys Rev L. 1983;50(17):1226–1229. doi: 10.1103/PhysRevLett.50.1226
[222] Blow KJ, Doran NJ. Global and local chaos in the pumped nonlinear Schrödinger equation. Phys Rev L. 1984;52(7):526–529. doi: 10.1103/PhysRevLett.52.526
[223] Wang Z, Hagerstrom A, Anderson JQ, et al. Chaotic spin-wave solitons in magnetic film feedback rings. Phys Rev L. 2011;107(11):114102. doi: 10.1103/PhysRevLett.107.114102
[224] Ustinov AB, Demidov VE, Kondrashov AV, et al. Observation of the chaotic spin-wave soliton trains in magnetic films. Phys Rev L. 2011;106(1):017201. doi: 10.1103/PhysRevLett.106.017201
[225] Haken H. Analogy between higher instabilities in fluids and lasers. Phys Rev L. 1975;53(1):77–78. doi: 10.1016/0375-9601(75)90353-9
[226] Yamada T, Graham R. Chaos in a laser system under a modulated external field. Phys Rev L. 1980;45(16):1322–1324. doi: 10.1103/PhysRevLett.45.1322
[227] Ruelle D, Takens F. On the nature of turbulence. In: Les Rencontres Physiciens-Mathématiciens de Strasbourg - RCP25. 1971;Vol. 12:1–44.
[228] Feigenbaum MJ. Quantitative universality for a class of nonlinear transformations. J Stat Phys. 1978;19(1):25–52. doi: 10.1007/BF01020332
[229] Pomeau Y, Manneville P. Intermittent transition to turbulence in dissipative dynamical systems. CMaPh. 1980;74:189–197. doi: 10.1007/BF01197757
[230] Zhao LM, Tang DY, Liu AQ. Chaotic dynamics of a passively mode-locked soliton fiber ring laser. Chaos. 2006;16(1):013128. doi: 10.1063/1.2173049
[231] Nielsen AU, Xu Y, Todd C, et al. Nonlinear localization of dissipative modulation instability. Phys Rev L. 2021;127(12):123901. doi: 10.1103/PhysRevLett.127.123901
[232] Zhang X, Zou D, Liu R, et al. From breather solitons to chaos in an ultrafast laser: The scenario of cascading short and long-period pulsations. Chaos, Solitons Fractals. 2024;182:114841. doi: 10.1016/j.chaos.2024.114841
[233] Lu X, Liu R, Guo M, et al. From breather soliton molecules to chaos in a laser cavity: the scenario of intermittent transitions. Opt Express. 2024;32(15):26207–26216. doi: 10.1364/OE.530009
[234] Duling IN. All-fiber ring soliton laser mode locked with a nonlinear mirror. Opt L. 1991;16(8):539–541. doi: 10.1364/OL.16.000539
[235] Hilborn RC. Chaos and Nonlinear Dynamics: An Introduction for Scientists and Engineers. Oxford, UK: Oxford University Press; 2000.
[236] Grassberger P, Procaccia I. Characterization of strange attractors. Phys Rev L. 1983;50(5):346–349. doi: 10.1103/PhysRevLett.50.346
[237] Lauterborn W, Cramer E. Subharmonic route to chaos observed in acoustics. Phys Rev L. 1981;47(20):1445–1448. doi: 10.1103/PhysRevLett.47.1445
[238] De Aguiar F, Rezende S. Observation of subharmonic routes to chaos in parallel-pumped spin waves in yttrium iron garnet. Phys Rev L. 1986;56(10):1070–1073. doi: 10.1103/PhysRevLett.56.1070
[239] Cartwright JH, González DL, Piro O. Universality in three-frequency resonances. Phys Rev E. 1999;59(3):2902–2906. doi: 10.1103/PhysRevE.59.2902

[240] Rossler OE. An equation for hyperchaos. Phys L A. 1979;71(2-3):157–159.
[241] Fischer I, Hess O, Elsäßer W, et al. High-dimensional chaotic dynamics of an external cavity semiconductor laser. Phys Rev L. 1994;73(16):2188–2191. doi: 10.1103/PhysRevLett.73.2188
[242] Pecora LM, Carroll TL. Synchronization in chaotic systems. Phys Rev L. 1990;64(8):821–824. doi: 10.1103/PhysRevLett.64.821
[243] Boccaletti S, Kurths J, Osipov G, et al. The synchronization of chaotic systems. Phys Rep. 2002;366(1–2):1–101. doi: 10.1016/S0370-1573(02)00137-0
[244] Wright LG, Christodoulides DN, Wise FW. Spatiotemporal mode-locking in multimode fiber lasers. Sci. 2017;358(6359):94–97. doi: 10.1126/science.aao0831
[245] Wright LG, Sidorenko P, Pourbeyram H, et al. Mechanisms of spatiotemporal mode-locking. Nat Phys. 2020;16(5):565–570. doi: 10.1038/s41567-020-0784-1
[246] Cao B, Gao C, Liu K, et al. Spatiotemporal mode-locking and dissipative solitons in multimode fiber lasers. Light: Sci Appl. 2023;12(1):260. doi: 10.1038/s41377-023-01305-0
[247] He WY, Liu GX, Zhang GX, et al. Periodically tunable multimode soliton pulsation in a spatiotemporal mode-locked fiber laser. Opt Express. 2024;32(3):4427–4435. doi: 10.1364/OE.510841
[248] Guo Y, Wen X, Lin W, et al. Real-time multispeckle spectral-temporal measurement unveils the complexity of spatiotemporal solitons. Nat Commun. 2021;12:67. doi: 10.1038/s41467-020-20438-z
[249] Guo Y, Lin W, Wang W, et al. Unveiling the complexity of spatiotemporal soliton molecules in real time. Nat Commun. 2023;14:2029. doi: 10.1038/s41467-023-37711-6
[250] Xiao X, Ding Y, Fan S, et al. Spatiotemporal period-doubling bifurcation in mode-locked multimode fiber lasers. ACS Photonics. 2022;9(12):3974–3980. doi: 10.1021/acsphotonics.2c01410
[251] Liu J, Guo Z, Wu X, et al. Real-time observation of breathing vortex solitons in a Yb: CALGO laser. Laser Photonics Rev. 2025;e01758.
[252] Chen R, Shu H, Shen B, et al. Breaking the temporal and frequency congestion of LiDAR by parallel chaos. Nat Photonics. 2023;17:306–314. doi: 10.1038/s41566-023-01158-4
[253] Lukashchuk A, Riemensberger J, Tusnin A, et al. Chaotic microcomb-based parallel ranging. Nat Photonics. 2023;17:814–821. doi: 10.1038/s41566-023-01246-5
[254] Jiang M, Wu H, An Y, et al. Fiber laser development enabled by machine learning: review and prospect. PhotoniX. 2022;3(1):16. doi: 10.1186/s43074-022-00055-3
[255] Ma Q, Yu H. Artificial intelligence-enabled mode-locked fiber laser: A review. Nan Me. 2023;6(1):36. doi: 10.1007/s41871-023-00216-3
[256] Boscolo S, Finot C. Artificial neural networks for nonlinear pulse shaping in optical fibers. Opt Laser Technol. 2020;131:106439. doi: 10.1016/j.optlastec.2020.106439
[257] Salmela L, Tsipinakis N, Foi A, et al. Predicting ultrafast nonlinear dynamics in fibre optics with a recurrent neural network. Nature Machine Intelligence. 2021;3:344–354. doi: 10.1038/s42256-021-00297-z
[258] Raissi M, Perdikaris P, Karniadakis GE. Physics-informed neural networks: A deep learning framework for solving forward and inverse problems involving nonlinear partial differential equations. J Comput Phys. 2019;378:686–707. doi: 10.1016/j.jcp.2018.10.045
[259] Zhakarov VE, Shabat AB. Exact theory of two-dimensional self-focusing and one-dimensional self-modulation of waves in nonlinear media. Sov Phys JETP. 1972;34(1):63–69.
[260] Wang Y, Li C, Chen F, et al. A prince for the sleeping beauty – NFT for soliton signal processing. Opt Commun. 2023;547:129857. doi: 10.1016/j.optcom.2023.129857
[261] Sugavanam S, Kopae MK, Peng J, et al. Analysis of laser radiation using the Nonlinear Fourier transform. Nat Photonics. 2019;10:5663.
[262] Sheveleva A, Hamdi S, Coillet A, et al. Analysis of the dispersive Fourier transform dataset using dynamic mode decomposition: evidence of multiple vibrational modes and their interplay in a three-soliton molecule. OptL. 2023;48:3015–3018. doi: 10.1364/OL.488968
[263] Sheveleva A, Coillet A, Finot C, et al. Langevin's model for soliton molecules in ultrafast fiber ring laser cavity: investigating experimentally the interplay between noise and inertia. Chaos, Solitons Fractals. 2025;197:116472. doi: 10.1016/j.chaos.2025.116472